Evaluation of Azido 3-Deoxy- d - Manno-oct-2-ulosonic Acid (Kdo) Analogues for Click Chemistry-Mediated Metabolic Labeling of Myxococcus xanthus DZ2 Lipopolysaccharide

Saïdi, Fares; Gamboa Marin, Oscar Javier; Veytia-Bucheli, José Ignacio; Vinogradov, Evgeny; Ravicoularamin, Gokulakrishnan; Jolivet, Nicolas Y.; Kezzo, Ahmad A.; Ramirez Esquivel, Eric; Panda, Adyasha; Sharma, Gaurav; Vincent, Stephane; Gauthier, Charles; Islam, Salim T.

Link to publication

Article

Evaluation of Azido 3-Deoxy-D-*manno*-oct-2-ulosonic Acid (Kdo) Analogues for Click Chemistry-Mediated Metabolic Labeling of *Myxococcus xanthus* DZ2 Lipopolysaccharide

Fares Saïdi, Oscar Javier Gamboa Marin, José Ignacio Veytia-Bucheli, Evgeny Vinogradov, Gokulakrishnan Ravicoularamin, Nicolas Y. Jolivet, Ahmad A. Kezzo, Eric Ramirez Esquivel, Adyasha Panda, Gaurav Sharma, Stéphane P. Vincent, Charles Gauthier,* and Salim T. Islam*

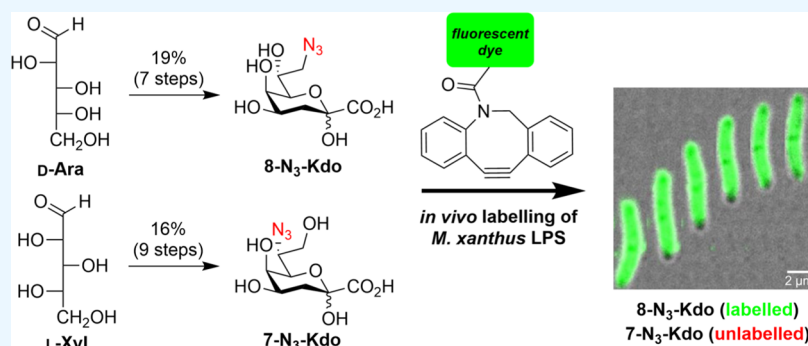Cite This: *ACS Omega* 2022, 7, 34997−35013

Read Online

| ACCESS | Metrics & More | Article Recommendations | Supporting Information |

ABSTRACT: Metabolic labeling paired with click chemistry is a powerful approach for selectively imaging the surfaces of diverse bacteria. Herein, we explored the feasibility of labeling the lipopolysaccharide (LPS) of *Myxococcus xanthus*—a Gram-negative predatory social bacterium known to display complex outer membrane (OM) dynamics—via growth in the presence of distinct azido (-N_3) analogues of 3-deoxy-D-*manno*-oct-2-ulosonic acid (Kdo). Determination of the LPS carbohydrate structure from strain DZ2 revealed the presence of one Kdo sugar in the core oligosaccharide, modified with phosphoethanolamine. The production of 8-azido-8-deoxy-Kdo (8-N_3-Kdo) was then greatly improved over previous reports via optimization of the synthesis of its 5-azido-5-deoxy-D-arabinose precursor to yield gram amounts. The novel analogue 7-azido-7-deoxy-Kdo (7-N_3-Kdo) was also synthesized, with both analogues capable of undergoing *in vitro* strain-promoted azide−alkyne cycloaddition (SPAAC) "click" chemistry reactions. Slower and faster growth of *M. xanthus* was displayed in the presence of 8-N_3-Kdo and 7-N_3-Kdo (respectively) compared to untreated cells, with differences also seen for single-cell gliding motility and type IV pilus-dependent swarm community expansion. While the surfaces of 8-N_3-Kdo-grown cells were fluorescently labeled following treatment with dibenzocyclooctyne-linked fluorophores, the surfaces of 7-N_3-Kdo-grown cells could not undergo fluorescent tagging. Activity analysis of the KdsB enzyme required to activate Kdo prior to its integration into nascent LPS molecules revealed that while 8-N_3-Kdo is indeed a substrate of the enzyme, 7-N_3-Kdo is not. Though a lack of *M. xanthus* cell aggregation was shown to expedite growth in liquid culture, 7-N_3-Kdo-grown cells did not manifest differences in intrinsic clumping relative to untreated cells, suggesting that 7-N_3-Kdo may instead be catabolized by the cells. Ultimately, these data provide important insights into the synthesis and cellular processing of valuable metabolic labels and establish a basis for the elucidation of fundamental principles of OM dynamism in live bacterial cells.

■ INTRODUCTION

The bacterial outer membrane (OM) serves as an important physical barrier, protecting the interiors of Gram-negative cells from the local environment.[1] The OM is thus often the first point of contact for extracellular interactions with other cells and/or substrata. Rather than a static structure, the OM is now known to be a highly dynamic interface, from which OM vesicle[2] and tube[3] projections are made, and for which its fluidity serves as a marker to activate stress-response pathways in a cell.[1]
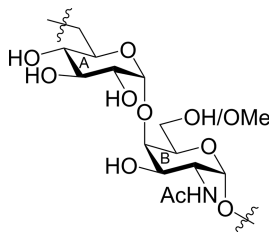
The OM is structured as an asymmetric bilayer, with the periplasmic (interior) leaflet largely composed of phospholipids. The outer leaflet is composed primarily of lip-

Table 1. NMR Spectroscopy Data for the *M. xanthus* DZ2 OAg[a]

Sugar	Nucleus	H/C 1	H/C 2	H/C 3	H/C 4	H/C 5	H/C 6
Glc (A)	^{1}H	4.92	3.53	3.81	3.54	4.24	3.63; 3.98
	^{13}C	101.8	73.2	73.9	70.7	72.4	66.8
GalNAc6OMe (B)	^{1}H	4.99	4.25	4.03	4.04	4.17	3.75; 3.82
	^{13}C	98.5	51.1	68.4	79.6	70.5	72.0
Glc (A')	^{1}H	4.97	3.55	3.81	3.54	4.24	3.63; 4.01
	^{13}C	101.8	73.2	73.9	70.7	72.4	66.8
GalNAc (B')	^{1}H	4.99	4.25	4.03	4.09	4.04	3.85; 3.90
	^{13}C	98.5	51.1	68.4	79.9	72.4	61.6

[a]Me at 3.41/59.7 ppm.

opolysaccharide (LPS), a glycolipid containing three distinct segments. The proximal portion of LPS is Lipid A, composed of two β-(1→4)-linked *N*-acetyl-2-deoxy-D-glucosamine residues to which attached acyl chains serve to embed LPS in the membrane. Molecules of LPS are also capped by a distal O-antigen (OAg) polymer, which contributes to antigenic serotyping specificity for diverse species. Finally, these two segments of LPS are linked via the core oligosaccharide (OS).[4] A unifying factor between Gram-negative species is the presence of 3-deoxy-D-*manno*-oct-2-ulosonic acid (Kdo) in the inner portion of the core OS, a sugar present in 1−4 copies depending on the species.[5] Following its synthesis, Kdo must first be processed by the cytidine monophosphate (CMP)-Kdo synthase KdsB; this enzyme catalyzes the activation of Kdo by addition of CMP (from cytidine triphosphate [CTP]) to the anomeric position of Kdo, allowing for downstream incorporation of this activated form of Kdo into nascent LPS molecules.[6−8]

Methods to label the bacterial OM have thus been developed to facilitate study of this dynamic cellular compartment via fluorescence microscopy.[9] A widespread method to visualize the OM is via treatment of intact cells with lipophilic fluorescent dyes that intercalate within the lipid bilayer. While quick and easy to use, such staining does not readily allow for distinction of labeling between the periplasmic and outer leaflets of the OM. Thus, the use of OM-targeted fluorescent proteins has also become a popular OM-labeling technology. Therein, fusion of a fluorescent protein such as mCherry or superfolder GFP (sfGFP)—capable of correctly folding in the periplasm—to an N-terminal OM lipoprotein sorting signal results in targeting of the fusion protein for insertion into the periplasmic leaflet of the OM and fluorescent labeling of the cell periphery. A benefit of such labeling is that it is genetically encoded and can thus be inducible or constitutive. However, localization of such constructs is confined to the periplasmic leaflet of the OM.

Bio-orthogonal click chemistry-mediated labeling of cell-surface LPS has emerged as a valuable addition to the OM-visualization toolbox. When grown in the presence of a synthetic Kdo variant elaborating an azido (-N$_3$) group at position 8 (8-N$_3$-Kdo), diverse Gram-negative species are able to take up the synthetic sugar, incorporate it within the core OS of nascent LPS molecules (in place of native Kdo), and successfully display this azido-modified LPS on the cell surface. Accessible azide groups in this metabolically labeled LPS can then be covalently reacted to a fluorophore-linked alkyne to undergo cycloaddition, thus fluorescently labeling the outer leaflet of the OM. Initially, Cu(I)-catalyzed azide−alkyne cycloaddition (CuAAC) was used to label cells elaborating 8-N$_3$-Kdo-containing LPS,[10] but this precluded further *in vivo* experimentation due to Cu(I)-induced cytotoxicity. To circumvent this limitation, strain-promoted azide−alkyne cycloaddition (SPAAC) has been subsequently employed to label 8-N$_3$-Kdo via click chemistry in the LPS of treated bacteria without killing the cells, thus permitting live-cell imaging of the OM.[11,12]

Gram-negative *Myxococcus xanthus* is a social bacterium with a multicellular life cycle. Within a swarm group, this bacterium exhibits coordinated behaviors of single cells. Conditions of nutrient depletion trigger the formation of aggregates in which cells are connected via OM tubes and chains of OM vesicles. These aggregates then mature into spore-filled fruiting bodies. Under such conditions, swarms also exhibit predatory behavior and can kill various bacteria and fungi to saprophytically utilize the degradation products. Groups of *M. xanthus* cells move via extension and retraction of type IV pili (T4P)[13] functioning in concert with secreted exopolysaccharide (EPS) and bio-surfactant polysaccharide (BPS),[13−15] whereas single cells glide on surfaces via substratum-coupling and directed transport of the Agl−Glt complex at bacterial focal adhesions.[16,17] Compatible *M. xanthus* cells can also fuse their cell envelopes and engage in OM exchange;[3] this phenomenon results in the transfer of OM contents that can transiently complement deficiencies in various OM proteins[18] and lipids.[19] All of the above complex physiological characteristics are linked by a requirement for a highly dynamic cell surface. To ultimately be able to study the *M. xanthus* cell surface in a selectively activable manner, we thus sought to evaluate the feasibility of metabolic labeling and bio-orthogonal click chemistry tagging of the OM in this bacterium.
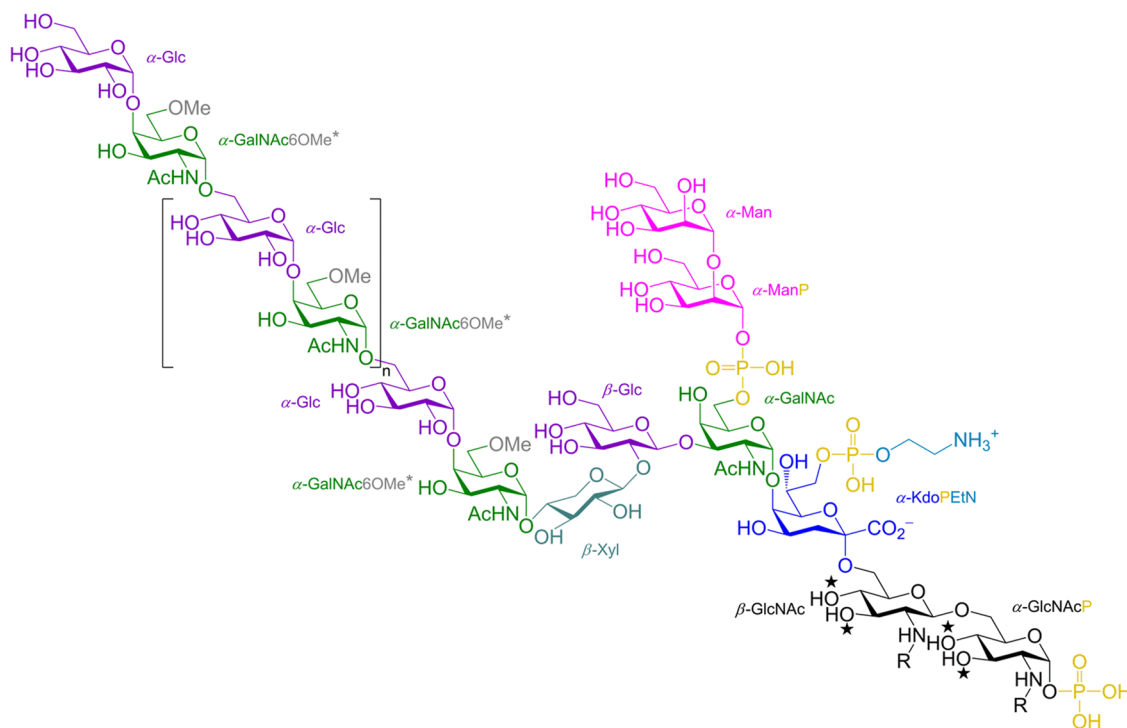
Figure 1. Schematic of the *M. xanthus* DZ2 LPS carbohydrate backbone. Lipid A amino groups are acylated (R) with 13-methyl-C_{14}-3OH, C_{16}-3OH, or 15-methyl-C_{16}-3OH fatty acids (in the ratio ~3:1:5) as previously reported.[20] However, the exact position of these fatty acids is not known. The acylation pattern of Lipid A −OH groups (★) was not determined herein.

Herein, we describe the structure of the *M. xanthus* DZ2 LPS carbohydrate backbone as well as novel syntheses of Kdo variants for click-mediated metabolic labeling with an azido group at position 8 (8-N_3-Kdo) or position 7 (7-N_3-Kdo) of the sugar. Cells incubated with 8-N_3-Kdo vs 7-N_3-Kdo, respectively, displayed slower vs faster growth (relative to untreated cells), but still displayed single-cell gliding motility, T4P-dependent group motility, and fruiting body formation. While both sugars demonstrated SPAAC reactivity *in vitro*, only the cell surfaces of 8-N_3-Kdo-grown live cells could be SPAAC-labeled with DBCO-linked fluorophores. While neither 8-N_3-Kdo or 7-N_3-Kdo were found to inhibit KdsB function, unlike the former, the latter was subsequently shown to not be processed by KdsB, precluding incorporation of 7-N_3-Kdo into nascent LPS molecules. Despite nonaggregating cells being shown to grow faster than those that do aggregate, cells grown in the presence or absence of 7-N_3-Kdo were found to aggregate at comparable rates, suggesting possible catabolism of 7-N_3-Kdo by cells. These data provide important insights into the syntheses and metabolic labeling of the bacterial OM with Kdo sugar azido derivatives, including the necessary processing of these sugars by recipient cells prior to their LPS integration.

RESULTS AND DISCUSSION

Structure of the *Myxococcus xanthus* DZ2 LPS Carbohydrate Backbone. To probe the appropriateness of OM metabolic labeling for *M. xanthus* DZ2, LPS was isolated from the bacterium via phenol−water treatment of WT cells followed by ultracentrifugation. Samples of LPS were hydrolyzed with 2% aqueous acetic acid and soluble products were separated via gel chromatography to yield OAg and core OS fractions.

^{1}H NMR analysis was carried out on the enriched *M. xanthus* DZ2 OAg polysaccharide, revealing a spectrum identical to the OAg of *M. xanthus* DK1622[20] (Figure S1A).

$$\rightarrow 6)-\alpha-\text{D}-\text{Glc}P-(1\rightarrow 4)-\alpha-\text{D}-\text{Gal}P\text{NAc6OMe}^*-(1\rightarrow$$
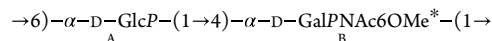
(A, B—with methyl group at B6, A′, B′—without methyl group)

This structure was confirmed via complete analysis of 2D NMR spectra (gCOSY, TOCSY, ROESY, HSQC, and HMBC) of OAg (Table 1). The methyl content of the OAg was calculated to be ~60% as determined via the integrals of ^{1}H signals of the methyl group at GalNAc O-6 and *N*-acetate. The NMR spectra of the OAg fraction contained many additional small signals, including some associated with a rhamnan, as identified via H-6 signals around 1.3/18 ppm (H/C).

Fractionated sample corresponding to *M. xanthus* DZ2 core OS was analyzed by negative-mode electrospray ionization (ESI)−mass spectrometry (MS). Observed peaks were found to fit the published structure of the core OS from *M. xanthus* DK1622[20] (Figure S1B)

$$\beta-\text{Xyl}-(1\rightarrow 2)-\beta-\text{Glc}-(1\rightarrow 3)-\alpha-\text{GalNAc6}PR-(1\rightarrow 5)-\text{Kdo8}P\text{EtN}$$
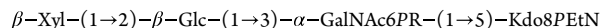
where R is α-Man-$(1\rightarrow 2)$-α-Man-1-(calculated exact mass 1244.31, observed *m/z* 1243.6) or H (exact mass 920.21, observed *m/z* 919.45). The peak at 787.4 corresponds to the loss of Xyl from 919.45. The content of α-Man-$(1\rightarrow 2)$-α-Man-1-disaccharide in the core OS from strain DZ2 was much lower than in DK1622.[20] With the presence of at least one Kdo sugar, the LPS of *M. xanthus* DZ2 (Figure 1) should thus be amenable to metabolic labeling with Kdo azido analogues.

Synthesis of 8-Azido-8-deoxy-Kdo (1), i.e., 8-N_3-Kdo. Given its high commercial price (>10 000 USD/g), we set out to optimize the in-house synthesis of 8-azido-8-deoxy-Kdo (**1**),
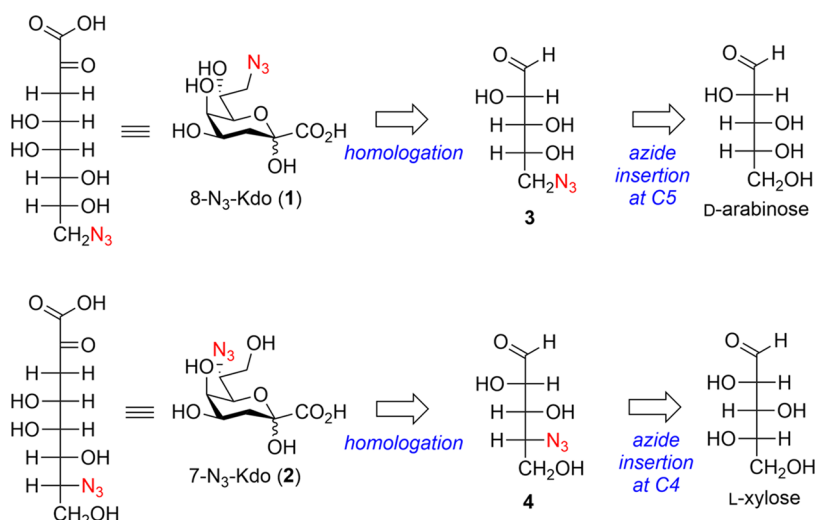
Figure 2. Retrosynthetic analyses of 8-N$_3$-Kdo (**1**) from D-arabinose, and 7-N$_3$-Kdo (**2**) from L-xylose.

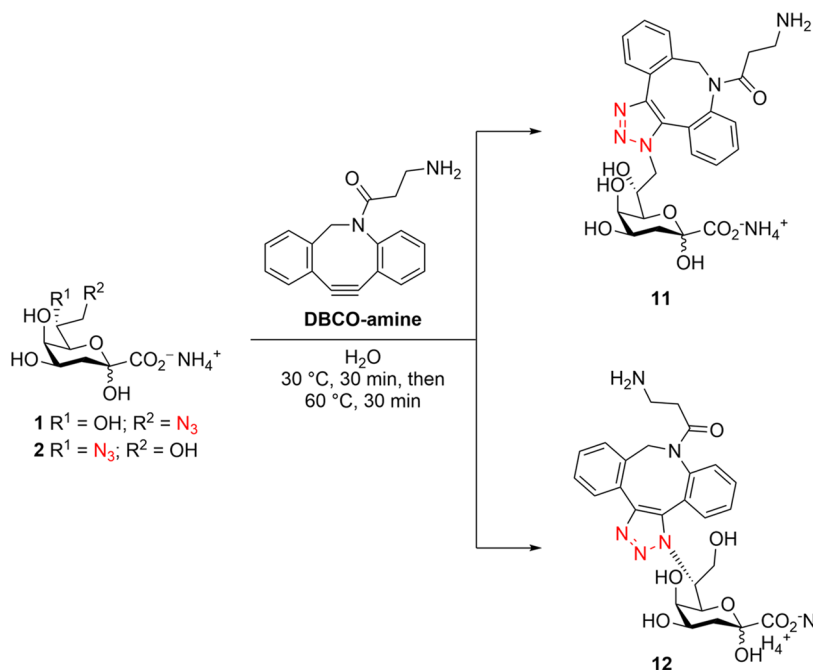## Scheme 1. Synthesis of 8-N$_3$-Kdo
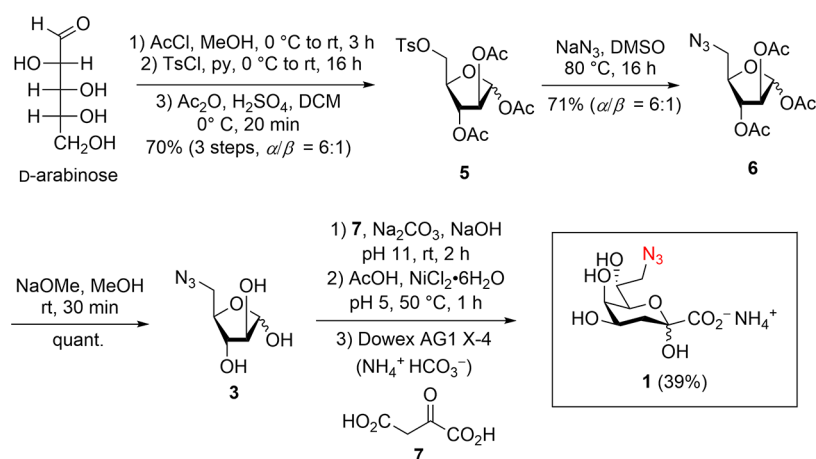
Scheme 2. Synthesis of 7-N$_3$-Kdo
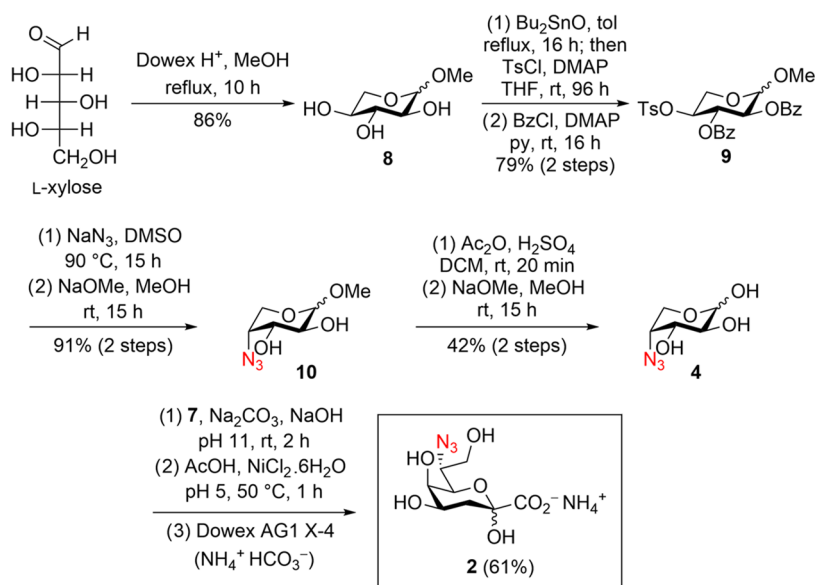
i.e., 8-N$_3$-Kdo, from 5-azido-5-deoxy-D-arabinose (**2**) (Figure 2), as previously outlined via the Cornforth homologation procedure.[10] To scale up the synthesis of 8-N$_3$-Kdo (**1**), we developed a straightforward procedure for the preparation of 5-

Scheme 3. SPAAC Reaction of DBCO-Amine with Either 8-N₃-Kdo or 7-N₃-Kdo

azido-5-deoxy-D-arabinose (**3**). As depicted in Scheme 1, commercially available D-arabinose was first subjected to a Fischer glycosylation using *in situ*-generated HCl from acetyl chloride and MeOH, followed by a regioselective tosylation of the hydroxyl group at the *O*-5 position. The corresponding tosylate was then submitted to acetolysis providing 1,2,3-tri-*O*-acetyl-5-*O*-tosyl-D-arabinofuranose (**5**) in good yield (70% over three steps) as a 6:1 α/β anomeric mixture.[21] Nucleophilic substitution of the tosylate group with sodium azide allowed us to access azide derivative **6** in good yield (71%, α/β ratio = 6:1).[21] Performing the azide substitution prior to the acetolysis step did not provide an improved reaction yield (25% over two steps). Zemplén deacetylation of azide **6** furnished the target precursor 5-azido-5-deoxy-D-arabinose (**3**) in quantitative yield. Our alternative procedure allowed us to prepare gram amounts of arabinose derivative (**3**) in an improved overall yield of 50% over five steps from D-arabinose and involved only two purification steps. In comparison, Kiefel's approach[22] toward 5-azido-5-deoxy-D-arabinose (**3**) was achieved in 35% yield over five steps and involved five purifications over silica gel. Azido-containing arabinose derivative **3** was finally transformed into the corresponding Kdo derivative through the Cornforth homologation procedure.[22] Therefore, condensation of derivative **3** with an excess of oxaloacetic acid (**7**) followed by NiCl₂-mediated decarboxylation[23] gave 8-azido-8-deoxy-Kdo (**1**) in 39% yield following anion exchange purification. Analytical data of 8-N₃-Kdo (**1**) agreed with those previously reported.[10,22]

Synthesis of 7-Azido-7-deoxy-Kdo (2), i.e., 7-N₃-Kdo. With the established presence of a *P*EtN modification at position 8 of native Kdo in *M. xanthus* LPS, we sought to synthesize a Kdo variant elaborating an azido group at a different position to potentially not impede *P*EtN addition. Similar to 8-N₃-Kdo, we planned to synthesize 7-azido-7-deoxy-Kdo (**2**), i.e., 7-N₃-Kdo, from 4-azido-4-deoxy-D-arabinose (**4**) via Cornforth homologation.[10,22] As depicted in our retrosynthetic analysis (Figure 2), azido-containing

derivative **4** would be obtained from L-xylose in which the azido group would be appended at the C4 position resulting in an inversion of configuration toward a D-arabinose derivative.

Our synthesis of 4-azido-4-deoxy-D-arabinose (**4**) was inspired by an approach developed by Kosma and co-workers[24] for 4-azido-containing L-arabinose derivatives. As shown in Scheme 2, commercially available L-xylose was first subjected to a Fischer glycosylation using Dowex H⁺ as the acid catalyst in refluxing MeOH. Accordingly, methyl L-xylopyranoside (**8**) was obtained in 86% yield as an inseparable α/β anomeric mixture. Tin acetal-mediated regioselective tosylation at the C4 position followed by benzoylation of the resulting diol at both C2 and C3 positions led to fully protected compound **9** in 79% yield after two steps. Importantly, attempts to use a nosyl (Ns) instead of a tosyl (Ts) group at the same position were not successful in our hands as only low yields of the target compound were obtained. S_N2 displacement reaction of the C4 tosylate by sodium azide in DMSO followed by Zemplén deacetylation provided D-arabinose derivative **10** in excellent yield (91% over two steps).¹H NMR analysis indicated that the pyranose ring was mainly found in the $^1C_4$ conformation ($^3J_{H1,H2}$ = 5.6 Hz for the major equatorial α-anomer). Compound **10** was then subjected to acetolysis by treatment with Ac₂O in the presence of H₂SO₄ leading to a triacetylated derivative, which was subsequently subjected to Zemplén saponification. The resulting 4-azido-4-deoxy-D-arabinose (**4**) was transformed into its corresponding 7-N₃-Kdo counterpart (**2**) using the Cornforth procedure (Scheme 2) in 61% yield following purification via anion exchange column.[22] NMR analysis showed that 7-N₃-Kdo (**2**) was found as a mixture of furanose and pyranose isomers with the α-pyranose as the major species.

8-N₃-Kdo and 7-N₃-Kdo Are Both Capable of Undergoing *In Vitro* SPAAC "Click" Reactions. To ensure the suitability of our synthesized 8-N₃-Kdo and 7-N₃-Kdo for use in metabolic labeling, we first probed the *in vitro* "click" reactivity of each synthesized sugar. Each of 8-N₃-Kdo and 7-N₃-Kdo was thus incubated with dibenzocyclooctyne
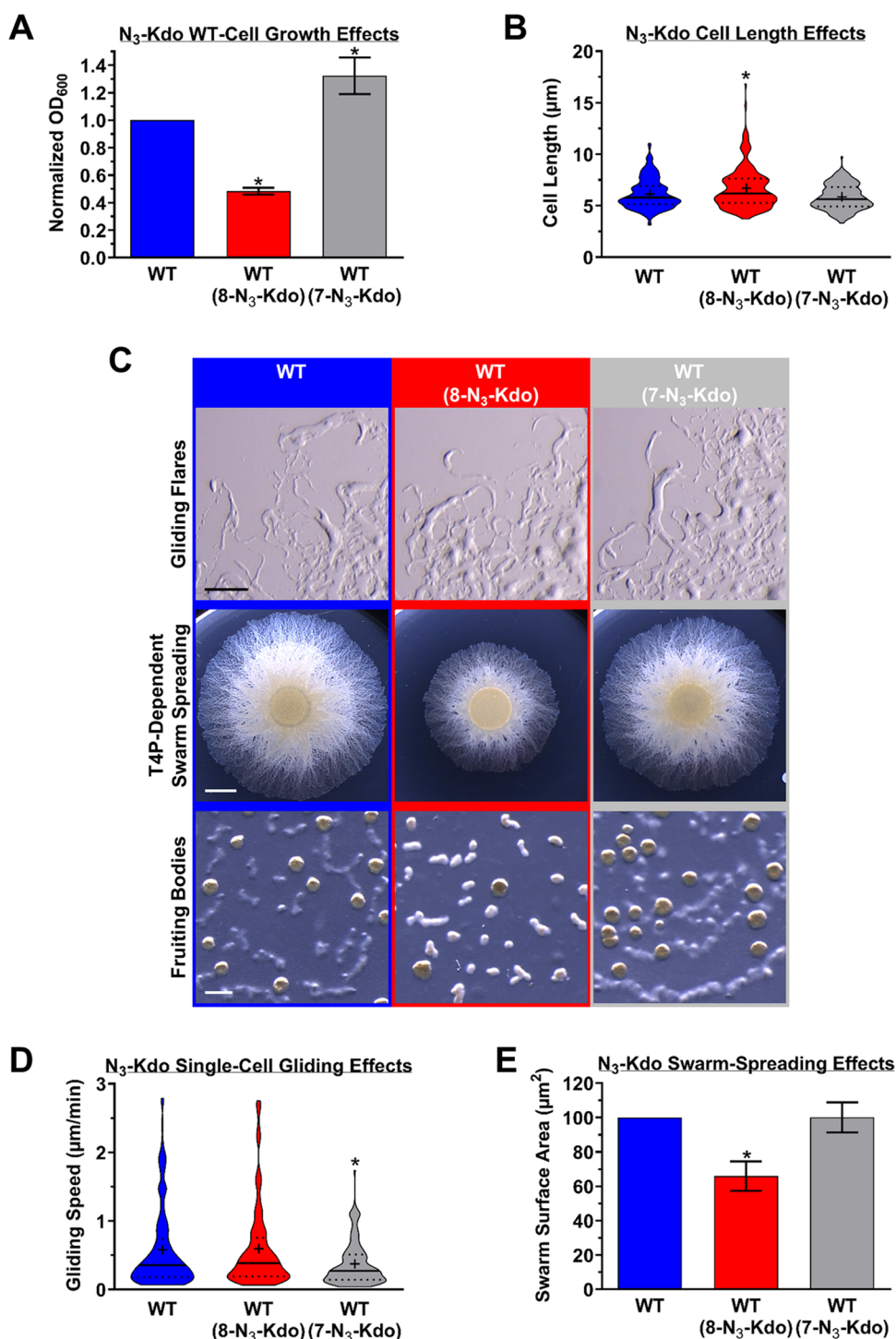
Figure 3. (A) Bar graph of normalized OD_{600} readings of WT *M. xanthus* DZ2 culture density following 24 h shaking incubation in the absence/ presence of 5 mM $8\text{-}N_3\text{-}Kdo$ or $7\text{-}N_3\text{-}Kdo$. For each biological replicate ($n = 7$), the value of the untreated culture was normalized to 1.0, with Kdo analogue-treated cultures normalized to the value of the untreated culture. Mean culture densities from those grown with either $8\text{-}N_3\text{-}Kdo$ or $7\text{-}N_3\text{-}Kdo$ were significantly different (*) from the untreated cultures, as evaluated via Student's *t*-test ($p < 0.05$). (B) Violin plots of lengths of cells grown in the absence/presence of Kdo azido analogues ($n = 184$ cells). Median (*solid lines*) and mean (+) as well as 25% and 75% quartile (*dotted lines*) values are indicated. $8\text{-}N_3\text{-}Kdo$-grown cells displayed a significantly different distribution of lengths (*) from untreated cells, as determined via two-tailed Mann−Whitney test ($p = 0.0303$). (C) *Top panels:* Gliding motility-dependent swarm-edge flares on CYE 1.5% agar at 56 h. Scale bar: 100 μm. *Middle panels:* T4P-dependent swarm expansion on CYE 0.5% agar at 72 h. Scale bar: 4 mm. *Bottom panels:* Fruiting body formation on CF 1.5% agar at 96 h. Scale bar: 2 mm. (D) Violin plots of single-cell gliding speeds ($n = 144$ cells). A gliding event was defined as minimum cell displacement equivalent to half the length of the cell. Median (*solid lines*) and mean (+) as well as 25% and 75% quartile (*dotted lines*) values are indicated. $7\text{-}N_3\text{-}Kdo$ cells displayed a significantly different distribution (*) from untreated as well as $8\text{-}N_3\text{-}Kdo$ cells, as determined via two-tailed Mann−Whitney test ($p < 0.05$). (E) Bar graph of mean swarm surface areas ($n = 3$). $8\text{-}N_3\text{-}Kdo$-grown cells displayed a significantly different mean value from either untreated or $7\text{-}N_3\text{-}Kdo$ cells, as evaluated via Student's t-test ($p < 0.05$).
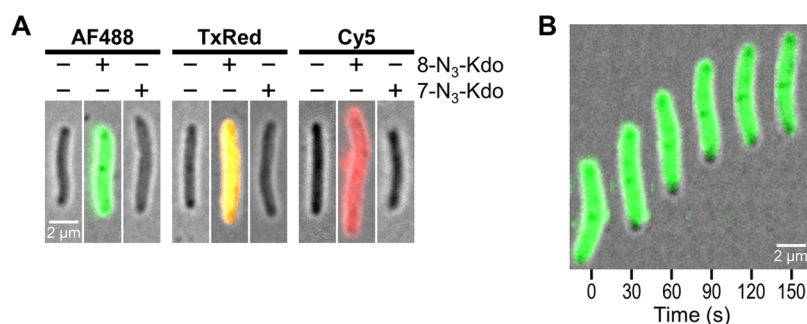
Figure 4. (A) Fluorescence micrographs of WT *M. xanthus* cells grown in the absence/presence of 8-N_3-Kdo or 7-N_3-Kdo and clicked with various DBCO-linked fluorophores (AF488, TxRed, Cy5). Images for each respective fluorophore were acquired with identical imaging settings and not adjusted in any way post-acquisition to show representative differences between treatments. (B) Fluorescent cell montage for a representative cell grown in 8-N_3-Kdo and clicked with DBCO-linked fluorophore (AF488), exhibiting gliding motility on a 1.5% agar pad. Cells remain viable even after all labeling and wash steps. Images were captured at 30 s intervals at 32 °C.

(DBCO)-amine under previously established[25] optimal SPAAC reaction conditions (30 °C for 30 min, then 60 °C for 30 min); this resulted in the formation of the expected adduct in each case after a total of 60 min of reaction (Scheme 3). The "click" reactivity of each sugar was next tested under conditions anticipated for *in vivo* labeling of *M. xanthus* cells, for which growth temperature is optimal at 32 °C. Both 8-N_3-Kdo and 7-N_3-Kdo were incubated with DBCO-amine for 1 h at 32 °C, with reaction aliquots removed at 5 min intervals. Thin-layer chromatography (TLC) analysis of the various aliquots indicated that the free sugars were already completely consumed after the first 5 min of the reaction (Figures S2 and S3). Each of the synthesized Kdo azido variants tested herein is thus capable of undergoing a SPAAC click reaction under idealized as well as *in vivo* labeling conditions.

8-N_3-Kdo and 7-N_3-Kdo Exert Different Growth Effects on *M. xanthus* Cells. To incorporate exogenous azido Kdo variants into nascent LPS molecules, broth cultures are typically supplemented with the desired sugar, allowing permissive bacteria to take up the exogenous sugar and incorporate it during their metabolic cycle.[10] Cells of WT *M. xanthus* DZ2 were thus grown in shaking cultures in the absence or presence of 8-N_3-Kdo or 7-N_3-Kdo. After 24 h of shaking incubation, WT cultures supplemented with 8-N_3-Kdo displayed ~52% slower growth relative to control cultures in which no sugar had been added. Conversely, WT growth in the presence of 7-N_3-Kdo was ~32% faster than in untreated cultures (Figure 3A). Importantly, measurements for cells from these cultures revealed comparable ranges of cell-body lengths, indicating no gross differences in morphology for cells subjected to any of the three treatments (Figure 3B). However, compared to untreated WT cells (median length: 5.797 μm), 8-N_3-Kdo-grown cells (median length: 6.207 μm) displayed a significantly different distribution of lengths, with values shifted toward slightly longer cells, representing a median increase of ~7.1% in the latter; conversely, the distribution of lengths for 7-N_3-Kdo-grown cells (median length: 5.642 μm) was determined to be comparable to that of untreated WT cells, with a median decrease of only ~2.7% (Figure 3B). Together, these data indicate that 8-N_3-Kdo and 7-N_3-Kdo exert different effects on WT *M. xanthus* cells.

Physiology of *M. xanthus* Cells Grown with 8-N_3-Kdo or 7-N_3-Kdo. For *M. xanthus* cells grown in the presence of 8-N_3-Kdo or 7-N_3-Kdo, we next sought to probe any deleterious effects on the complex multicellular life cycle of the bacterium. Despite the different doubling times of cells grown in broth

supplemented with either Kdo analogue (Figure 3A), once spotted on a solid 1.5% "hard" agar matrix, the production of macroscopic swarm-edge flares was intact for both 8-N_3-Kdo- and 7-N_3-Kdo-grown cells (Figure 3C); this suggests that individual cells are still capable of exhibiting gliding motility. Phase-contrast microscopy imaging and single-cell motility tracking on agar pads revealed that gliding speeds were equivalent between WT cells grown in the absence and presence of 8-N_3-Kdo, but significantly slower in 7-N_3-Kdo-grown cells (Figure 3D). As untreated and 7-N_3-Kdo-grown cells were of comparable lengths (Figure 3B), this may point to differences in gliding machinery activation and/or function stemming from potential differences in the metabolic states of these cells.

On a soft 0.5% agar substratum, swarms of 7-N_3-Kdo-grown WT cells spread as well as native WT swarms, indicating that T4P-dependent motility of cell groups was not compromised for cells having undergone this treatment (Figure 3C,E). Conversely, T4P-dependent swarm spreading was partially inhibited in 8-N_3-Kdo-grown WT cells (Figure 3C,E). If 8-N_3-Kdo is indeed incorporated into *M. xanthus* LPS, this may indicate a role for *P*EtN (attached to native Kdo at position 8) in T4P-dependent swarm biofilm spreading.

Finally, under nutrient-limiting conditions, the ability of cells from either treatment to aggregate and contribute to fruiting body formation was maintained, indicating the continued capacity of these cells to undertake a developmental cycle (Figure 3C). Taken together, these results indicate that Kdo azido variants are compatible with the complex life cycle of *M. xanthus*.

Surfaces of *M. xanthus* Cells Grown in 8-N_3-Kdo vs 7-N_3-Kdo Are Differentially Labeled. To probe the click reactivity of LPS from cells grown in 8-N_3-Kdo and 7-N_3-Kdo, cells grown in either sugar were treated with DBCO-linked fluorescent dyes, namely (i) AFDye 488 (DBCO-AF488), (ii) polyethylene glycol (PEG)$_4$-5/6- Texas Red (DBCO-TxRed), and (iii) Cy5 (DBCO-Cy5). This was done in an effort to fluorescently label cell-surface LPS elaborating exposed -N_3 groups via a SPAAC click reaction. As evidenced via live-cell fluorescence microscopy, cells grown in the presence of 8-N_3-Kdo displayed bright fluorescent peripheral marking with all three DBCO-linked fluorophores, indicative of successfully click-labeled LPS in these cells (Figure 4A). Importantly, these cells were still motile following the various click and wash steps, demonstrating their continued viability (Figure 4B). Unexpectedly, cells from 7-N_3-Kdo-supplemented cultures
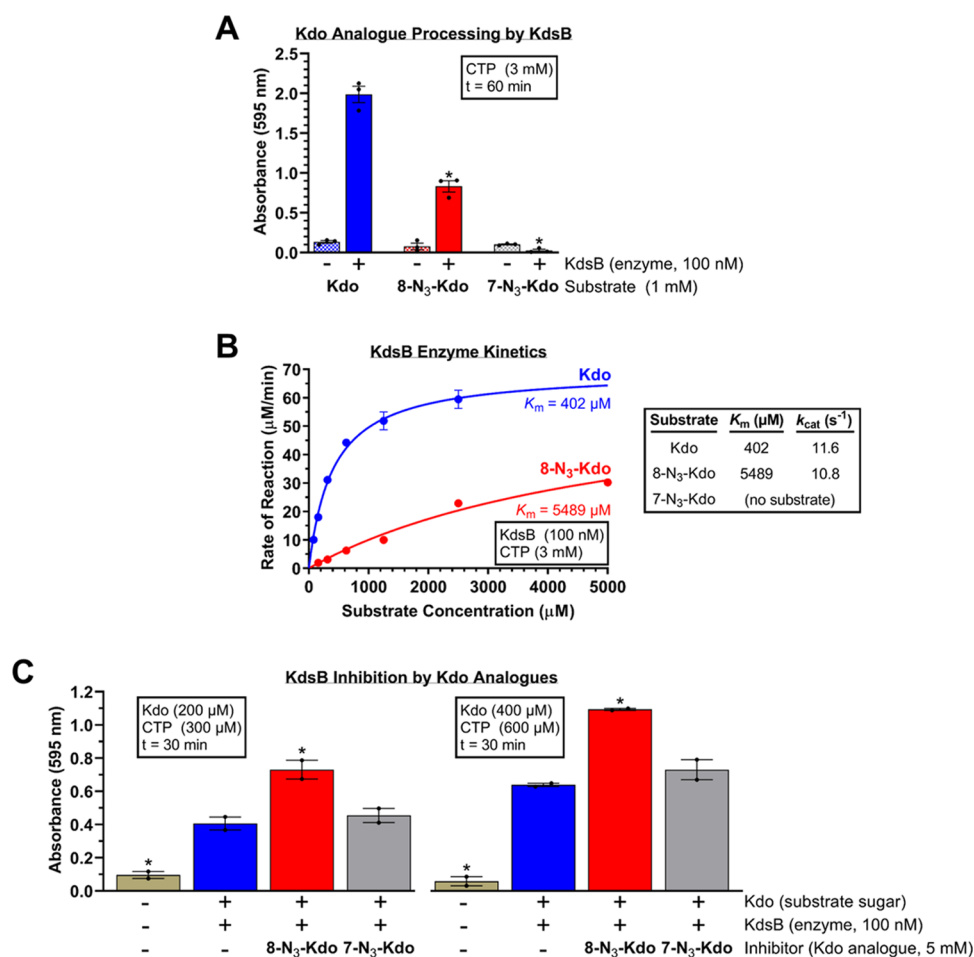
Figure 5. (A) KdsB substrate suitability. Mean values from three experimental replicates ($\pm$SEM) for PPi release by KdsB (measured via A_{595}) with Kdo are significantly different from those of KdsB with 8-N_3-Kdo or 7-N_3-Kdo, as determined via unpaired two-tailed Student's t-test ($p < 0.001$). (B) KdsB enzyme kinetics in the presence of native Kdo or various azido analogues. Mean values from three experimental replicates ($\pm$SEM) are indicated. (C) KdsB inhibition assay using Kdo azido analogues. Mean values from two experimental replicates ($\pm$SEM) for PPi release by KdsB (measured via A_{595}) with Kdo. Compared to reference "KdsB + Kdo"-alone samples, those also containing 8-N_3-Kdo, as well as those lacking either component displayed significant differences, as determined via unpaired two-tailed Student's *t*-test ($p < 0.05$).

treated with any of the three DBCO-linked dyes did not display any peripheral fluorescence (Figure 4A), despite the *in vitro* SPAAC reactivity of 7-N_3-Kdo (Figure S3); this suggests that 7-N_3-Kdo is not taken up by cells and/or cannot be incorporated into LPS.

***M. xanthus* Encodes Numerous Major Facilitator Superfamily Proteins.** Both *E. coli* and *Klebsiella pneumoniae* were previously shown to be permissive for metabolic labeling via 8-N_3-Kdo incorporation, with both species known to contain the *nan* sialic acid uptake operon, whereas native *Pseudomonas aeruginosa*, which does not contain the *nan* operon, could not be so labeled. Specific expression of sialic acid transporter NanT—a major facilitator superfamily (MFS) protein—was shown to mediate 8-N_3-Kdo transport across the IM into the cytoplasm in *E. coli*; moreover, heterologous expression of *E. coli* NanT in *P. aeruginosa* resulted in the latter cells being metabolically labeled with 8-N_3-Kdo.[26] Given the role of MFS transporter NanT in mediating Kdo azido-analogue uptake, we thus scanned the *M. xanthus* genome[27] for NanT homologues as well as proteins containing known Pfam domains MFS_1, MFS_1_like, MFS_2, MFS_3, MFS_4, and MFS_5. This analysis revealed 36 putative MFS transporter proteins encoded by the bacterium (Table S1). Previous

RNAseq transcriptomic profiling[28,29] revealed these genes to be expressed during the *M. xanthus* life cycle (Table S1). While identification of the specific transporter gene(s) responsible for Kdo azido-variant uptake is beyond the scope of the current paper, these data are consistent with diverse transport capabilities for *M. xanthus*, which are reflective of its broad metabolic capacity as a soil bacterium.

8-N_3-Kdo (But Not 7-N_3-Kdo) Is a Substrate for CMP-Kdo Synthase KdsB. Given the requirement for Kdo to be processed into an activated form by KdsB prior to its incorporation into LPS[6−8]—via the addition of CMP (from CTP), releasing pyrophosphate [PP_i] in the process—we thus carried out an enzymatic assay to determine the suitability of 8-N_3-Kdo and 7-N_3-Kdo as substrates for KdsB. In the presence of CTP, KdsB was incubated with either Kdo, 8-N_3-Kdo, or 7-N_3-Kdo, with ensuant PP_i release quantified via chromogenic reaction with eikonogen reagent followed by spectrophotometric determination of absorbance at 595 nm.[30] Kdo and 8-N_3-Kdo were shown to be substrates for KdsB, with the latter more inefficiently processed; conversely, 7-N_3-Kdo could not be processed by the enzyme under these conditions (Figure 5A). We then forced the experimental conditions to an even greater extent to see if 7-N_3-Kdo was indeed a substrate,
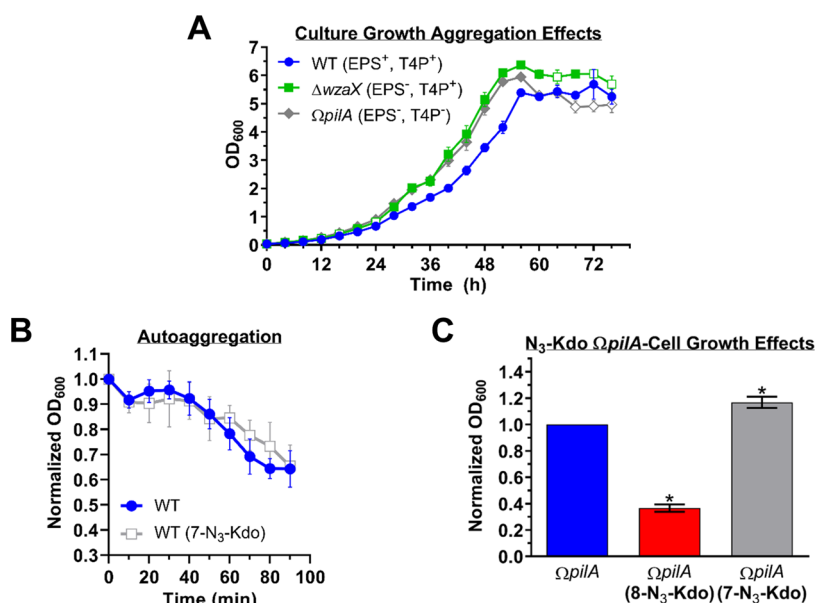
Figure 6. (A) Growth comparison for WT *M. xanthus* DZ2 compared to the nonaggregating isogenic $\Delta wzaX$ and $\Omega pilA$ mutant strains. Cultures were inoculated at an initial OD_{600} of 0.05, grown with shaking incubation at 32 °C for 86 h, with OD_{600} readings taken at 4 h intervals. Values represent mean OD_{600} values ±SEM of seven biological replicates. Statistical significance for each mutant value relative to WT was calculated using a mixed-effects model with Geisser−Greenhouse correction and Dunnett's multiple comparisons test ($p < 0.05$). (B) Autoaggregation profiles of WT cells grown in the absence or presence of 7-N_3-Kdo. Values represent mean OD_{600} values ±SEM of three biological replicates. Statistical significance for each mutant value relative to WT was calculated using a two-way ANOVA with Sidak's multiple comparisons test ($p < 0.05$). Legend for Panels A and B: *solid plot points*, statistically significant difference in mutant/treatment values relative to untreated WT at a given time point; *open plot points*, no statistically significant difference between mutant/treated strain and WT values. (C) Bar graph of normalized OD_{600} readings of *M. xanthus* DZ2 $\Omega pilA$ culture density following 24 h shaking incubation in the absence or presence of 5 mM 8-N_3-Kdo or 7-N_3-Kdo. For each biological replicate ($n = 4$), the value of the untreated culture was normalized to 1.0, with 8-N_3-Kdo- or 7-N_3-Kdo-grown cultures normalized to the value of the untreated culture. Mean culture densities from those grown with either 8-N_3-Kdo or 7-N_3-Kdo were significantly different (*) from the untreated cultures, as evaluated via unpaired two-tailed Student's *t*-test ($p < 0.05$).

increasing its concentration to 5000 μM (up to ∼12× the K_M for Kdo) and the reaction time up to 3 h. However, no reaction was observed (Figure 5A). The lack of KdsB activity toward 7-N_3-Kdo may indicate that the hydroxyl group at C7 of Kdo plays a crucial role in the interaction of Kdo with KdsB. Alternatively, the presence of a bulkier -N_3 group at C7 of Kdo may not allow 7-N_3-Kdo to properly situate in the binding pocket of KdsB[31] (as opposed to Kdo with a -N_3 group at C8 which can likely extend further into the open cavity) (Figure S4), indicating that the enzyme may be more permissive to Kdo modifications at C8 versus C7.

Using varying concentrations of Kdo, 8-N_3-Kdo and 7-N_3-Kdo (0−5000 μM), we determined the steady-state kinetic parameters of purified KdsB in the presence of each sugar (via monitoring of PP_i release as described above), with the enzyme displaying Michaelis−Menten parameters in the presence of Kdo and 8-N_3-Kdo (as per previous reports[30,32]); no PP_i release was detected in the presence of 7-N_3-Kdo (Figure 5B). However, native Kdo still proved to be a more efficient acceptor for CMP compared to 8-N_3-Kdo (Figure 5B).

Since each Kdo azido variant was not processed by KdsB to the extent of native Kdo, the inhibitory potential for each analogue on KdsB was tested. KdsB was first preincubated with high concentrations of 8-N_3-Kdo or 7-N_3-Kdo (5000 μM), after which substrate mix was added containing CTP and native Kdo at concentrations set at ∼0.5 and 1 K_M to favor the detection of substrate competitors. After incubation for 30 min, reactions were quenched with ethanol, followed by detection of released PP_i. Under these conditions, neither of the Kdo azido analogues had an inhibitory effect on KdsB

(Figure 5C). For 8-N_3-Kdo in particular, as it is a substrate for KdsB (Figure 5A,B), an even larger amount of PPi was released into the reaction mixture (compared to native Kdo alone) (Figure 5C), suggesting that KdsB is capable of interchangeably metabolizing both Kdo and 8-N_3-Kdo.

The lack of surface click labeling with DBCO-linked fluorophores for 7-N_3-Kdo-grown cells (Figure 5A) is consistent with an inability of this particular Kdo azido analogue to be processed by KdsB, thus precluding its incorporation into nascent LPS molecules. This is likely a broadly applicable finding given the extensive sequence conservation between KdsB proteins from diverse proteobacteria, in particular with respect to key active-site residues implicated in Kdo processing[31] (Figure S5).

7-N_3-Kdo May Be Catabolized by *M. xanthus* Cells. Within the context of 7-N_3-Kdo not being incorporated into LPS molecules (Figure 4), we thus revisited the faster growth phenotype of *M. xanthus* DZ2 grown in the presence of this Kdo azido analogue. Conventional wisdom in working with *M. xanthus* holds that nonaggregating strains grow faster than those that aggregate. To explicitly test this assertion, we compared the growth curves of WT *M. xanthus* DZ2 in liquid culture with those of the nonaggregating[13] isogenic mutant strains $\Delta wzaX$ (deficient in EPS secretion) and $\Omega pilA$ (deficient in T4P assembly and EPS secretion). Both $\Delta wzaX$ and $\Omega pilA$ were found to achieve exponential-phase growth, and reach stationary phase, sooner than WT (Figure 6A), consistent with a lack of *M. xanthus* cell aggregation resulting in faster culture growth. We thus compared the auto-aggregative profiles[13] of WT cells grown in the absence and

presence of 7-N$_3$-Kdo to probe for reduced clumping in the latter. However, cells grown with 7-N$_3$-Kdo clumped and sedimented in cuvettes at comparable rates to untreated cells (Figure 6B), indicating that altered aggregation was not a viable explanation for accelerated growth in the presence of 7-N$_3$-Kdo. To support this contention, we compared the growth of the nonaggregating[13] Ω*pilA* mutant strain of *M. xanthus* in the absence/presence of Kdo azido analogues. Similar to WT cells (Figure 3A), Ω*pilA* cells grew ∼63% slower in the presence of 8-N$_3$-Kdo (Figure 6C). Importantly, Ω*pilA* mutant cells also grew ∼17% faster in the presence of 7-N$_3$-Kdo compared to untreated cells (analogous to WT cells) (Figure 6C), despite their inability to aggregate.[13] Therefore, the higher density of *M. xanthus* cells in the presence of 7-N$_3$-Kdo may be due to catabolism of this particular supplemented Kdo azido variant resulting in accelerated growth.

■ CONCLUSIONS

We reported the first-ever synthesis of a Kdo variant with a substitution at carbon 7, 7-azido-7-deoxy-Kdo (7-N$_3$-Kdo), in addition to greatly improving the synthesis of 8-azido-8-deoxy-Kdo (8-N$_3$-Kdo). The eight-carbon skeleton of these Kdo analogues was efficiently built via the Cornforth homologation procedure from the corresponding azido-containing D-arabino precursors, opening an efficient synthetic route to the more cost-effective generation of modified Kdo sugars.

Cells of *M. xanthus* grown with 8-N$_3$-Kdo exhibited slower growth. However, given the capacity of these cells to manifest a multicellular life cycle, this would suggest that depletion of *P*EtN within the context of the bacterium's total cell-surface Kdo pool is not overly deleterious to the viability of the bacterium. However, the depletion of -*P*EtN groups and/or the non-native presence of -N$_3$ groups deep in the inner core OS would be expected to modify the overall cell-surface properties to a certain degree, which may help explain various phenotypic differences (Figure 3). As cases-in-point, cells with different physical surface properties display differences in single-cell gliding speeds, gliding reversal frequencies, dye-binding profiles, tolerance to antibiotics and oxidative-stress agents, and biofilm organization, as well as T4P formation, stability, and positioning.[13,14,33]

The effect of 7-N$_3$-Kdo is more perplexing. While it clearly cannot be detected on the cell surface (given its inability to be processed by KdsB and thus not activated for integration into an LPS molecule), in its presence, aggregating and non-aggregating strains alike grew faster than untreated cells. Cells grown with 7-N$_3$-Kdo also exhibited slower single-cell gliding motility, despite being of equivalent length to untreated cells. As cell-surface LPS should be identical between WT cells grown with and without 7-N$_3$-Kdo, the overall cell-surface properties between such samples should be comparable. Therefore, differences in cell-surface properties are an unlikely explanation for altered gliding speed. This may instead point to an as-yet-unknown metabolic effect that affects the production and/or function of the gliding motility machinery. Considering this and the faster growth in the presence of 7-N$_3$-Kdo (a phenotype that is not due to decreased aggregation), this may point to 7-N$_3$-Kdo being used as an energy source by the cells, thus favoring cell growth. Such a contention does however require further investigation to more concretely support it.

The X-ray crystal structure of KdsB may provide insights into the ability of the enzyme to process 8-N$_3$-Kdo, but not 7-N$_3$-Kdo. Although a -N$_3$ at Kdo carbon 8 would extend upward

into the cavity of the binding pocket, a -N$_3$ at Kdo carbon 7 would likely abut against the wall of the binding pocket, disfavoring the required stereochemistry at the active site (Figure S4). Functional Kdo analogues (i.e., those that can be processed by KdsB and have CMP added) have been previously shown with modifications at carbon 3, 5, or 8.[34] Given that CMP is added to carbon 2, and considering the unoccupied space in the binding pocket (Figure S4), carbon 4 may also support a −N$_3$ modification without impeding addition of CMP.

Ultimately, our data provide important insights into the improved synthesis of valuable metabolic labels and establish a basis for the elucidation of fundamental principles of OM dynamism in bacteria.

■ METHODS

General Synthesis Methods. All of the starting materials and reagents were purchased from commercial sources and used without further purification. Air- and water-sensitive reactions were conducted in oven-dried glassware under an inert atmosphere in anhydrous solvents, which were prepared by supplying the solvents over heat-gun activated 4 Å molecular sieves. These solvents were introduced to the reaction through a dried, argon-filled syringe. Reactions were monitored by TLC with silica gel 60 F$_{254}$ 0.25 mm precoated aluminum foil plates. Compounds were visualized using UV$_{254}$ and orcinol (1 mg·mL^{-1}) in a 10% aqueous solution of H$_2$SO$_4$ or Hanessian's stain [2 g of Ce(SO$_4$)$_4$(NH$_4$)$_4$, 5 g of MoO$_4$(NH$_4$)$_2$, 200 mL of H$_2$O, and 20 mL of H$_2$SO$_4$] with heating. Normal-phase flash column chromatography was performed on silica gel 60 Å (15−40 μm). Reversed-phase flash column chromatography was performed on C$_{18}$ silica gel (fully capped, 25−40 μm). Anion exchange column chromatography was performed on Serdolit CG-400 I (Cl$^-$ form). NMR spectra were recorded at 297 K in the mentioned deuterated solvents with 400 or 600 MHz instruments, employing standard software given by the manufacturer. ^{1}H and ^{13}C NMR spectra were referenced to TMS ($\delta_H = \delta_C = 0.00$ ppm) and acetone ($\delta_H = 2.22$ ppm; $\delta_C = 30.9$ ppm) for spectra in D$_2$O. Assignments were based on ^{1}H, ^{13}C, HSQC, and COSY experiments. All of the ^{13}C NMR experiments were ^{1}H-decoupled. High-resolution mass spectra (HRMS) were recorded on an ESI-Q-TOF mass spectrometer. All NMR analyses for molecule verifications have been provided (Figures S6−S33)

Synthesis of 1,2,3-Tri-O-acetyl-5-O-tosyl-D-arabinofuranose (5). D-Arabinose (2.0 g, 13.3 mmol, 1.0 equiv) was suspended in MeOH (48 mL) at 0 °C. A freshly prepared solution of AcCl (1.1 mL, 15.5 mmol, 1.16 equiv) in MeOH (9.5 mL) at 0 °C was added dropwise to the latter suspension. The mixture was warmed up to rt and stirred for 3 h at rt. TLC analysis (DCM/MeOH 8:2) showed full conversion of the starting material. The reaction was then quenched with pyridine (4 mL), and the resulting mixture was co-evaporated with toluene. The crude was then dissolved in dry pyridine (41 mL) under argon at 0 °C. A solution of TsCl (3.8 g, 20.0 mmol, 1.5 equiv) in anhydrous pyridine (41 mL) was then added dropwise. The mixture was warmed up to rt and stirred for 16 h. After verification of the complete consumption of the starting material by TLC (100% EtOAc), the reaction was quenched by adding ice water (3 g) and stirring for 30 min. Water (50 mL) was added, and the aqueous phase was extracted with EtOAc (3 × 50 mL). The organic layers were

combined, washed with brine (25 mL), and dried over MgSO$_4$. The solvents were evaporated under reduced pressure. The resulting crude was then dissolved in dry DCM (80 mL) under argon. Ac$_2$O (12.6 mL, 133 mmol, 10 equiv) was added, and the mixture was cooled down to 0 °C. Concentrated H$_2$SO$_4$ (710 μL, 13.3 mmol, 1.0 equiv) was added dropwise. The mixture was stirred at 0 °C for 20 min. TLC analysis (100% EtOAc) showed total conversion of the starting material. The reaction mixture was poured on a mixture of ice/water (100 mL). DCM was then evaporated under reduced pressure. The resulting aqueous phase was extracted with EtOAc (3 × 100 mL). The organic phases were combined, washed with a saturated aqueous solution of NaHCO$_3$ (2 × 75 mL), dried over MgSO$_4$, and the solvents were evaporated under reduced pressure. The crude was then purified by silica gel column chromatography (100% hexanes to hexanes/EtOAc 5:5) to give compound **5** (4.0 g, 70% over three steps, α/β = 6:1) as a pale yellow oil. Analytical data agreed with those previously reported.[21]

Synthesis of 1,2,3-Tri-O-acetyl-5-azido-5-deoxy-D-arabinofuranose (6). A solution of compound **5** (3.2 g, 7.5 mmol, 1.0 equiv) and NaN$_3$ (1.84 g, 28.4 mmol, 3.8 equiv) in dry DMSO under argon was stirred at 80 °C for 16 h. After verification of the consumption of the starting material by TLC (hexanes/acetone 6:4), the reaction mixture was diluted with DCM (100 mL). The organic phase was washed with H$_2$O (2 × 100 mL), dried over MgSO$_4$, and the solvents were evaporated under reduced pressure. The crude was then purified by silica gel column chromatography (hexanes/EtOAc 8:2 to 4:6) to give compound **6** (1.6 g, 71%, α/β = 6:1) as a pale yellow oil. Analytical data agreed with those previously reported.[21]

Ammonium 8-Azido-3,8-dideoxy-D-manno-oct-2-ulopyranosylonate (1). To a solution of compound **6** (455 mg, 1.51 mmol, 1.0 equiv) in MeOH (9.4 mL) was added a 25% w/w solution of NaOMe in MeOH (65.3 μL, 0.3 mmol, 0.2 equiv). The resulting mixture was stirred at rt for 30 min. TLC analysis (DCM/MeOH 9:1) showed full conversion of the starting material. The reaction was then quenched by the addition of Dowex H$^+$ resin until pH ≈ 7 was reached. The suspension was then filtered over Celite and the solvents were evaporated under reduced pressure to give 5-azido-5-deoxy-D-arabinose (3), which was directly used in the next step without further purification. Azide **3** (265 mg, 1.5 mmol, 1.0 equiv) was dissolved in distilled H$_2$O (4.5 mL) containing Na$_2$CO$_3$ (394 mg, 3.7 mmol, 2.5 equiv). Oxaloacetic acid (242 mg, 1.8 mmol, 1.2 equiv) was added in small portions over 5 min. After adding a few drops of a 10 N aqueous NaOH solution until the pH increased to 11.0 (as checked with a pH meter), the reaction mixture was stirred at rt for 2 h. Then, the pH was decreased to 5.0 using AcOH. Catalytic NiCl$_2$·6H$_2$O (0.01 equiv) was added and the mixture was stirred at 50 °C for 1 h. Then, the pH was increased again to 8.0 with a saturated aqueous solution of NH$_4$OH. After cooling the mixture to rt, it was passed through an anion exchange resin column CG-400 (HCO$_3^-$). It was first eluted with H$_2$O to remove the excess of azide **3** and then eluted with aqueous NH$_4$HCO$_3$ (0.05 N to 0.30 N). The fractions were pooled according to TLC analysis (CHCl$_3$/MeOH/H$_2$O 10:10:3 as revealed with Hanessian's stain) and freeze-dried to provide ammonium Kdo derivative **1** (163 mg, 39%) as a white amorphous solid. Analytical data agreed with those previously reported.[10,22]

Synthesis of Methyl L-Xylopyranoside (8). L-Xylose (1.0 g, 6.7 mmol, 1.0 equiv) was dissolved in anhydrous MeOH (200 mL) under Ar at rt. Dowex H$^+$ resin (500 mg) was added, and the mixture was refluxed for 16 h. The reaction mixture was cooled down to rt and then filtered over Celite. The solvents were evaporated under reduced pressure. The residue (anhydrous loaded) was purified through silica gel flash chromatography (DCM/MeOH/acetone 16.5:0.5:3.0 to 14:3:3) to give methyl xylopyranoside **8** (921 mg, 86%, α/β = 5:3) as a pale yellowish powder: R_f 0.3 (DCM/MeOH/acetone 7.0:1.5:1.5); ^{1}H NMR (600 MHz, MeOD, α-anomer) δ 4.61 (d,$^3J_{1,2}$ = 3.7 Hz, 1H, H-1), 3.57-3.52 (m, 2H, H-3, H-5a), 3.47−3.40 (m, 2H, H-4, H-5b), 3.38 (s, 3H, OCH$_3$), 3.36 (dd,$^3J_{2,3}$ = 9.5 Hz,$^3J_{1,2}$ = 3.7 Hz, 1H, H-2); ^{13}C NMR (150 MHz, MeOD, α-anomer) δ 100.2 (C1), 73.8 (C4), 72.2 (C2), 70.1 (C3), 61.4 (C5), 54.2 (OCH$_3$); HRMS (ESI-TOF) m/z [M + Na]$^+$ calculated for C$_6$H$_{12}$O$_5$ 187.0577; found 187.0571.

Synthesis of Methyl 2,3-Di-O-Benzoyl-4-O-tosyl-L-xylopyranoside (9). A Dean-stark apparatus was fixed to a flask in which Bu$_2$SnO (1.4 g, 5.7 mmol, 1.1 equiv) and methyl xylopyranoside **8** (921 mg, 5.6 mmol, 1.0 equiv) were suspended in anhydrous toluene (18 mL). After the mixture was refluxed for 6 h, it was cooled down to rt and the solvents were evaporated under reduced pressure. To a solution of this residue in anhydrous THF (8.4 mL), a solution of TsCl (1.3 g, 6.8 mmol, 1.2 equiv) in anhydrous THF (11 mL) was added dropwise under Ar in the presence of DMAP (1 mg, 5 μmol, 0.001 equiv) and left to stir at rt for 96 h. Following reaction completion according to TLC (100% EtOAc), the solvents were evaporated under reduced pressure. The residue (dry-loaded) was purified using silica gel flash chromatography. First, the column was eluted with toluene to remove most of the dibutyltin salts, and then with the eluent system (100% EtOAc) to give methyl 4-O-para-toluenesulfonyl-α-L-xylopyranoside contaminated with tin salts. The latter crude diol was dissolved in anhydrous pyridine (17.5 mL) under Ar. After cooling the mixture to 0 °C, BzCl (2.0 mL, 18 mmol, 3.1 equiv) was added dropwise followed by DMAP (7.1 mg, 0.058 mmol, 0.01 equiv). The reaction mixture was warmed to rt and stirred for 16 h. After reaction completion according to TLC (hexanes/EtOAc 5:5), it was diluted with EtOAc (50 mL). The organic phase was washed with a 1 N aqueous HCl solution (2 × 50 mL), followed by a saturated aqueous NaHCO$_3$ solution (50 mL), and then with brine (50 mL). The organic layers were dried using MgSO$_4$ and then evaporated under reduced pressure. The resulting residue was purified by silica gel flash chromatography (hexanes/EtOAc 9:1 to 6:4) to give derivative **9** (2.3 g, 79% over 2 steps, α/β = 5:2) as a white amorphous solid: R_f 0.4 (hexanes/EtOAc 6:4); ^{1}H NMR (600 MHz, CDCl$_3$, α-anomer) δ 7.91−7.87 (m, 2H, H-Ar), 7.73−7.66 (m, 2H, H-Ar), 7.63−7.61 (m, 2H, H-Ar), 7.52−7.45 (m, 2H, H-Ar), 7.34−7.31 (m, 4H, H-Ar), 6.99−6.91 (m, 2H, H-Ar), 5.94-5.86 (m, 1H, H-3), 5.09−5.02 (m, 2H, H-1, H-2), 4.67 (ddd,$^3J_{4,5b}$ = 11.0 Hz,$^3J_{3,4}$ = 7.0 Hz,$^3J_{4,5a}$ = 6.1 Hz, 1H, H-4), 4.06 (dd,$^2J_{5a,5b}$ = 11.2 Hz,$^3J_{4,5a}$ = 6.1 Hz, 1H, H-5a), 3.41 (dd,$^2J_{5a,5b}$ = 11.0 Hz,$^3J_{4,5b}$ = 11.0 Hz, 1H, H-5b), 3.41 (s, 3H, OCH$_3$), 2.16 (s, 3H, CH$_3$-Ar); ^{13}C NMR (100 MHz, CDCl$_3$, α-anomer) δ 165.7, 165.0 (2 × CO), 144.8, 133.4 133.1, 129.9, 129.8, 129.8, 129.8, 129.7, 129.7, 128.4, 128.5, 128.1, 127.6 (C-Ar), 96.8 (C-1), 75.7 (C-4), 71.8 (C-2), 69.2 (C-3) 59.2 (C-5), 55.6 (OCH$_3$), 21.6 (CH$_3$-Ar); HRMS (ESI-TOF) m/z [M + Na]$^+$ calculated for C$_{27}$H$_{26}$NaO$_9$S 549.1195; found 549.1202.

Synthesis of Methyl 4-Azido-4-deoxy-D-arabinopyrano-side (10). To a solution of derivative **9** (17.5 g, 33.3 mmol, 1.0 equiv) in anhydrous DMSO (50 mL), NaN$_3$ (8.1 g, 125 mmol, 2.5 equiv) was added, and the mixture was stirred under Ar at 90 °C overnight. Then, the reaction mixture was diluted with DCM (200 mL) and the organic phase was washed with distilled water (2 × 100 mL) and a saturated aqueous NaHCO$_3$ solution (100 mL). The organic layer was dried using MgSO$_4$, and the solvents were evaporated under reduced pressure. The resulting residue was purified by silica gel flash chromatography (hexanes/EtOAc 7:3 to 1:1) to provide methyl 4-azido-2,3-di-*O*-benzoyl-4-deoxy-D-arabinopyranoside (**S1**, 14.0 g, quantitative, α/β = 3.5:1.5) as a white amorphous solid: R_f 0.3 (hexanes/acetone 6:3); ^{1}H NMR (600 MHz, CDCl$_3$, α-anomer) δ 8.06−7.97 (m, 6H, C*H*-Ar), 7.57−7.52 (m, 2H, C*H*-Ar), 7.44−7.40 (m, 4H, C*H*-Ar), 5.59−5.56 (m, 1H, H-2), 5.51 (dd,$^3J_{2,3}$ = 7.9 Hz,$^3J_{3,4}$ = 3.3 Hz, 1H, H-3), 4.60 (d,$^3J_{1,2}$ = 5.6 Hz, 1H, H-1), 4.20−4.16 (m, 2H, H-5a, H-4), 3.80 (m, 1H, H-5b), 3.50 (s, 3H, OCH$_3$); ^{13}C NMR (100 MHz, CDCl$_3$, α-anomer) δ 165.8, 165.2 (2 × CO), 133.7, 133.5, 130.2, 129.9, 129.4, 128.9, 128.6, 128.5 (C-Ar), 101.2 (C-1), 71.6 (C-3), 69.3 (C-2), 61.9 (C-5), 57.7 (C-4), 56.6 (CH$_3$). HRMS (ESI-TOF) m/z [M + Na]$^+$ calculated for C$_{20}$H$_{19}$N$_3$O$_6$ 420.1166; found 420.1174. To a solution of the latter azide (13 g, 33 mmol, 1.0 equiv) in anhydrous DCM/MeOH (1:6 *v/v*, 350 mL) was added a NaOMe solution (25 wt % in MeOH, 1.5 mL, 6.5 mmol, 0.2 equiv), and the reaction was stirred overnight under Ar at rt. The reaction mixture was quenched by adding Dowex H$^+$ resin until neutrality was reached. The resin was filtered through Celite and the solvents were evaporated under reduced pressure. The residue was purified by silica gel flash chromatography (DCM/MeOH 1:0 to 92:8) to give diol **10** (5.66 g, 91%, α/β 10:1) as a white amorphous solid: R_f 0.4 (DCM/MeOH 9:1); ^{1}H NMR (600 MHz, D$_2$O, α-anomer) δ 4.27 (d,$^3J_{1,2}$ = 7.7 Hz, 1H, H-1), 4.05−4.02 (m, 1H, H-5a), 4.00−3.98 (m, 1H, H-4), 3.89 (dd,$^3J_{2,3}$ = 9.5 Hz,$^3J_{3,4}$ = 4.0 Hz, 1H, H-3), 3.73 (dd,$^2J_{5a,5b}$ = 13.2 Hz,$^3J_{4,5b}$ = 1.5 Hz, 1H, H-5b), 3.54 (s, 3H, OCH$_3$), 3.51−3.48 (m, 1H, H-2); ^{13}C NMR (100 MHz, D$_2$O, α-anomer) δ 104.0 (C-1), 72.3 (C-3), 70.8 (C-2), 63.8 (C-5), 61.5 (C-4), 57.1 (CH$_3$); HRMS (ESI-TOF) m/z [M + Na]$^+$ calculated for C$_6$H$_{11}$N$_3$NaO$_4$ 212.0642; found 212.0644.

Synthesis of 4-Azido-4-deoxy-D-arabinopyranose (4). To a solution of diol **10** (5.2 g, 27 mmol, 1.0 equiv) dissolved in DCM (275 mL), Ac$_2$O (26 mL, 275 mmol, 10.0 equiv) was added and the reaction mixture was cooled down to 0 °C. A solution of concentrated H$_2$SO$_4$ (1.5 mL, 27 mmol, 1.0 equiv) was added, and the reaction was warmed to rt and stirred for 20 min. After diluting the mixture with DCM (50 mL), the organic phase was washed with a saturated aqueous NaHCO$_3$ solution (3 × 100 mL) and brine (100 mL). The combined organic layers were dried over MgSO$_4$, and the solvents were evaporated under reduced pressure. The residue was purified by silica gel flash chromatography (hexanes/EtOAc 8:2 to 1:1) to give 1,2,3-tri-*O*-acetyl-4-azido-4-deoxy-D-arabinopyranoside (**S2**, 3.8 g, 50%, α/β 1.5:3.5) as a white amorphous solid: R_f 0.3 (Hex/EtOAc 6:4); ^{1}H NMR (600 MHz, CDCl$_3$, β-anomer) δ 6.31 (d,$^3J_{1,2}$ = 3.0 Hz, 1H, H-1), 5.41−5.36 (m, 2H, H-2, H-3), 4.18-4.14 (m, 1H, H-4), 4.07−4.03 (m, 1H, H-5a, H5aβ), 3.82 (dd,$^2J_{5a,5b}$ = 12.7 Hz,$^3J_{4,5b}$ = 2.2 Hz Hz 1H, H-5b), 2.15 (s, 3H, COCH$_3$), 2.14 (s, 3H, COCH$_3$), 2.04 (s, 3H, COCH$_3$); ^{13}C NMR (100 MHz, CDCl$_3$, β-anomer) δ 170.4, 169.8, 169.1 (3 × COCH$_3$), 90.2 (C-1), 69.2, (C-3), 66.7 (C-

2), 62.5 (C-5), 59.4 (C-4), 21.0, 20.7, 20.7 (3 × COCH$_3$); HRMS (ESI-TOF) m/z [M + Na]$^+$ calculated for C$_{11}$H$_{15}$N$_3$NaO$_7$ 324.0802; found 324.0810. The latter derivative (3.8 g, 13 mmol, 1.0 equiv) was dissolved in anhydrous DCM/MeOH (1:4 *v/v*, 125 mL), a NaOMe solution was added (25 wt % in MeOH, 577 μL, 2.52 mmol, 0.2 equiv), and the reaction was stirred overnight at rt. The reaction mixture was quenched with Dowex H$^+$ resin until neutrality was reached. The resin was filtered off through Celite and the solvents were evaporated under reduced pressure. The residue was purified by reversed-phase (C$_{18}$) silica gel flash chromatography (H$_2$O/ACN 1:0 to 75:25) to give target derivative **4** (2.0 g, 91%, α/β 1:1) as white amorphous solid: R_f 0.2 (DCM/MeOH 9:1); ^{1}H NMR (600 MHz, D$_2$O) δ 5.22 (d,$^3J_{1,2}$ = 3.7 Hz, 1H, H-1α), 4.51 (d,$^3J_{1,2}$ = 7.8 Hz, 1H, H-1β), 4.10−4.06 (m, 2H, H-3α, H-5aα), 4.03 (m, 1H, H-4α), 4.00−3.96 (m, 2H, H-4β, H5aβ), 3.87 (dd,$^3J_{3,2}$ = 9.7 Hz,$^3J_{3,4}$ = 3.9 Hz, 1H, H-3β), 3.78 (dd,$^3J_{2,3}$ = 9.8 Hz,$^3J_{2,1}$ = 3.7 Hz, 1H, H-2α), 3.75 − 3.70 (m, 2H, H-5bα, H-5bβ), 3.47 (dd, 1H,$^3J_{2,3}$ = 9.7 Hz,$^3J_{2,1}$ = 7.8 Hz); ^{13}C NMR (600 MHz, D$_2$O) δ 96.8 (C-1β), 92.5 (C-1α), 72.5 (C-3β), 71.9 (C-2β), 68.6 (C-3α), 68.5 (C-2α), 63.9 (C-5β), 62.1 (C-4α), 61.7 (C-4β), 60.0 (C-5α); HRMS (ESI-TOF) m/z [M + Na]$^+$ calculated for C$_5$H$_9$N$_3$NaO$_4$ 198.0485; found 198.0480.

Ammonium 7-Azido-3,7-dideoxy-D-manno-oct-2-ulopyr-anosylonate (2). Azide **4** (350 mg, 2.0 mmol, 1.0 equiv) was dissolved in distilled H$_2$O (6.0 mL) containing Na$_2$CO$_3$ (526 mg, 4.9 mmol, 2.5 equiv). Oxaloacetic acid (317 mg, 2.4 mmol, 1.2 equiv) was added in small portions over 5 min. After adding a few drops of a 10 N aqueous NaOH solution until the pH increased to 11.0 (as checked with a pH meter), the reaction mixture was stirred at rt for 2 h. Then, the pH was decreased to 5.0 using AcOH, catalytic NiCl$_2$·6H$_2$O (0.01 equiv) was added, and the mixture was stirred at 50 °C for 1 h. After cooling the mixture to rt, it was passed through an anion exchange resin column CG-400 (HCO$_3$$^-$). It was first eluted with H$_2$O to remove the excess of azide **4** and then eluted with aqueous NH$_4$HCO$_3$ (0.05 to 0.30 N). The fractions were pooled according to TLC analysis (CHCl$_3$/MeOH/H$_2$O 10:10:3; revealed with Hanessian's stain) and freeze-dried to provide ammonium Kdo derivative **2** (340 mg, 61%) as a white amorphous solid. According to NMR, compound **2** was obtained as a mixture of *furano* and *pyrano* anomers with α-pyranose as the major form. $[\alpha]_D^{20}$ = +0.67 (*c* 0.90, H$_2$O); ^{1}H NMR (600 MHz, D$_2$O, α-pyranose anomer) δ 3.91 (ddd,$^3J_{4,3a}$ = 12.1 Hz,$^3J_{4,3b}$ = 5.2 Hz,$^3J_{4,5}$ = 3.1 Hz, 1H, H-4), 3.87-3.80 (m, 2H, H-7, H-8a), 3.69-3.61 (m, 2H, H-5, H-6), 3.57 (dd,$^2J_{8b,8a}$ = 12.0 Hz,$^3J_{8b,7}$ = 6.0 Hz 1H, H-8b), 1.83 (d,$^2J_{3a,3b}$ = 13.0 Hz,$^3J_{3a,4}$ = 12.1 Hz, 1H, H-3a), 1.73 (dd,$^2J_{3b,3a}$ = 13.0 Hz,$^3J_{3b,4}$ = 5.2 Hz, 1H, H-3b); ^{13}C NMR (100 MHz, D$_2$O, α-pyranose anomer) δ 177.2 (C-1), 97.2 (C-2), 70.6 (C-6), 67.7 (C-7), 66.6 (C-4), 62.6 (C-5), 62.0 (C-8), 33.2 (C-3); HRMS (ESI-TOF) m/z [M − H]$^-$ calculated for C$_8$H$_{12}$N$_3$O$_7$ 262.0686; found 262.0675.

Click Reaction for 8-Azido-8-deoxy-Kdo (1) and 7-Azido-7-deoxy-Kdo (2) with DBCO-amine. Click reactions were performed using a method described by Bharathi and co-workers[25] (Scheme 3) in which the azido derivative (3.0 mg, 11 μmol, 1.0 equiv) and DBCO-amine (3.0 mg, 11 μmol, 1.0 equiv) were dissolved in water (160 μL). The mixture was stirred at 30 °C for 30 min, then at 60 °C for 30 min. TLC (CHCl$_3$/MeOH/H$_2$O 10:10:3) showed total conversion of the starting material in both cases (**1** and **2**) to yield click

derivatives **11** and **12**. The crude was finally freeze-dried, and the residue was directly analyzed by HRMS. HRMS (ESI-TOF): for compound **11** m/z [M]$^-$ calculated for $C_{26}H_{28}N_5O_8^-$ 538.1943; found 538.1932; for compound **12** m/z [M]$^-$ calculated for $C_{26}H_{28}N_5O_8^-$ 538.1943; found 538.1942.

Bacterial Cell Culture. *M. xanthus* DZ2 was cultured in CYE (10% w/v Bacto Casitone peptone, 5% w/v yeast extract, 1% w/v MgCl$_2$, 10 mM MOPS [pH 7.4]) broth with shaking (220 rpm), or on CYE solidified with 1.5% agar, at 32 °C. To obtain sufficient biomass for LPS structure determination, 10 g of lyophilized cells from shaking CYE liquid cultures (grown at 32 °C) were harvested via centrifuge (7000 × g, 15 min).

For metabolic labeling with 8-N$_3$-Kdo and 7-N$_3$-Kdo, 1 mL CYE cultures (in 28 mL glass tubes) were supplemented with 5 mM (i.e., 25 μL of a 200 mM stock solution prepared with sterile ddH$_2$O) of either Kdo azido variant. Each tube was then inoculated with *M. xanthus* DZ2 (WT or Ω*pilA* [TM293]) at an initial OD$_{600}$ of 0.02. Tubes were closed with sliding plastic caps, with the caps sealed to the tubes using Parafilm. Culture tubes were then inclined on a tube rack and incubated with shaking for 24 h. To remove culture rings accumulating on the side of the glass tubes, tubes were briefly mixed via vortex every 6−8 h to dissociate the adhered ring and ensure cells remained in the liquid phase. Upon harvest, 100 μL of culture volume was diluted in 900 μL of TPM to help dissociate clumps, followed by reading of the OD$_{600}$ in a disposable polystyrene cuvette to determine the final culture density using a spectrophotometer.

Growth Curve Analysis. Wild-type (DZ2),[35] Δ*wzaX* (TM469),[36] and Ω*pilA* (TM293)[13] strains were initially grown overnight in 12.5 mL CYE cultures in a shaking incubator (32 °C, 220 rpm, 125 mL flask). The next day, each strain was subcultured into a 150 mL CYE starting volume (in a 1 L flask) to a starting OD$_{600}$ of 0.05, and grown for 86 h (32 °C, 220 rpm). Culture density was measured every 4 h via determination of the OD$_{600}$. Prior to cultures reaching an OD$_{600}$ of 1.0, 1 mL of culture volume was removed at each time point and transferred to a disposable spectrophotometer cuvette; cuvettes were then inserted into foam microtube racks, floated in a Bransonic 32 Ultrasonic cleaner bath (Branson), sonicated for 30 s to break up cell aggregates, after which OD$_{600}$ was determined. At each time point following culture attainment of an OD$_{600}$ of 1.0, 100 μL of culture was transferred to a cuvette, and diluted with 900 μL of TPM buffer (10 mM Tris-HCl, pH 7.6, 8 mM MgSO$_4$, and 1 mM KH$_2$PO$_4$), prior to sonication and OD$_{600}$ determination as described.

Extraction of LPS for Backbone and OAg Structure Determination. LPS was extracted by stirring 2−3 g of lyophilized cell mass in 200 mL of 45% aqueous phenol at 75 °C for 20 min. The ensuing mixture was dialyzed for several days in running tap water, after which acetic acid was added to 10% final concentration. The precipitate was then removed by centrifugation at 8000 rpm for 30 min, followed by dialysis against distilled water and lyophilization. This freeze-dried sample was then dissolved in 10 mL of ddH$_2$O, after which AcOH was added to a final concentration of 2%. The sample was heated for 2 h at 100 °C until clear solution and precipitate formed, then cooled. The precipitate was removed by centrifugation at 10 000 rpm, followed by product separation on a Biogel P6 column (2.5 × 60 cm^2) in 1% aqueous AcOH, then lyophilized.

To prepare OAg for structure determination, LPS was hydrolyzed by 2% aqueous AcOH (100 °C, 1−2 h, until a precipitate was formed). The precipitate was removed by centrifugation and then separated on a Biogel P6 column (2.5 × 60 cm^2) in 1% aqueous AcOH with a refractive index detector.

Gel Chromatography. Gel chromatography was performed on a Sephadex G-15 column (1.5 × 60 cm^2) or a Biogel P6 column (2.5 × 60 cm^2) in 1% aqueous acetic acid, monitored by a refractive index detector (Gilson).

Anion Exchange Chromatography. Sample up to 50 mg was injected into a HiTrap Q column (Amersham, two columns, by 5 mL each, connected in series) in water at 3 mL·min^{-1}, washed with water for 5 min, and then eluted with a linear gradient from water to 1 M aqueous NaCl over 1 h with UV detection at 220 nm and spot test on silica TLC plate with development by dipping in 5% H$_2$SO$_4$ in ethanol and heating with heat gun until brown spots become visible. Samples were desalted on Sephadex G-15 column (1.6 × 60 cm^2) in 1% aqueous AcOH with a refractive index detector.

NMR Spectroscopy for LPS Structure Determination. For LPS structure determination, NMR experiments were carried out on a Bruker AVANCE III 600 MHz (^{1}H) spectrometer with 5 mm Z-gradient probe with acetone internal reference (2.225 ppm for ^{1}H and 31.45 ppm for ^{13}C) using standard pulse sequences cosygpprqf (gCOSY), mlevphpr (TOCSY, mixing time 120 ms), roesyphpr (ROESY, mixing time 500 ms), hsqcedetgp (HSQC), hsqcetgpml (HSQC-TOCSY, 80 ms TOCSY delay), and hmbcgplpndqf (HMBC, 100 ms long-range transfer delay). The resolution was kept <3 Hz/pt in F2 in proton−proton correlations and <5 Hz/pt in F2 of H−C correlations. The spectra were processed and analyzed using the Bruker Topspin 2.1 program. Monosaccharides were identified by COSY, TOCSY, and NOESY cross-peak patterns and ^{13}C NMR chemical shifts. Amino group location was concluded from high-field signal position of aminated carbons (CH at 45−60 ppm). Connections between monosaccharides were determined from transglycosidic NOE and HMBC correlations.

Mass Spectrometry for LPS Structure Determination. For LPS analysis, ESI-MS was obtained using a Waters SQ Detector 2 instrument. Samples were injected in 50% aqueous MeCN with 0.1% TFA. Cone voltage was set to 60 V for nondestructive MS or to 160 V to observe fragmentation of polymers.

Determination of Neutral and Amino Sugars as Alditol Acetates. Monosaccharides were detected as reduced and acetylated derivatives (alditol acetates). Polysaccharide sample (0.2−1.0 mg) with inositol internal standard was hydrolyzed with 3 M aqueous TFA (120 °C, 3 h), dried, reduced with NaBD$_4$, reagent-destroyed with 0.5 mL of AcOH, solution-dried under the stream of air, dried twice with the addition of MeOH (1 mL), acetylated with 0.2 mL of Ac$_2$O and 0.2 mL of pyridine for 30 min at 100 °C, dried, and analyzed by GC-MS on Thermo Trace 1310 instrument with ITQ1100 ion trap detector, capillary column HP-5, 160−260 °C by 4 °C·min^{-1}.

Phenotypic Analyses. For cultures grown in glass tubes, cells were sedimented via centrifuge (4000 × g, 5 min) and resuspended in TPM buffer to an OD$_{600}$ of 2.0, followed by spotting 5 μL of each resuspension to the appropriate matrix and incubation at 32 °C of the Parafilm-sealed plate. To analyze gliding motility flare formation, cells were spotted to

15 cm × 15 cm Petri plates containing CYE 1.5% agar (BD Difco) and grown for 56 h. To probe T4P-dependent swarm spreading, the cells were spotted on CYE 0.5% agar plates and incubated for 72 h. Fruiting body formation under nutrient-minimal conditions was examined on CF (1 mM MOPS [pH 7.6], 1 mM KH_2PO_4 [pH 7.6], 8 mM $MgSO_4$, 0.015% Casitone w/v) 1.5% agar plates after 96 h.

Phenotype plates were imaged on an Olympus SZX16 stereoscope with ILLT base. To image gliding flares, objective 2× and zoom 8× were used with illumination between the oblique and brightfield lenses. T4P-dependent swarm spreading was captured at objective 0.5×, zoom 0.7×, with dark-field illumination. Fruiting bodies were imaged using objective 0.5×, zoom 2×, with oblique illumination. Measurements of T4P-dependent swarm surface area were obtained using Olympus CellSens software with the three-point circle method.

SPAAC "Click" Chemistry Labeling of Cells Grown with Kdo Azido Variants. For cultures grown in glass tubes with Kdo azido variants, the calculated culture volume was removed and sedimented in a centrifuge ($4000 \times g$, 5 min) so that resuspension in 10 μL would yield an OD_{600} of 1.0. Cell pellets were then twice washed with TPM buffer and sedimented ($4000 \times g$, 5 min). Pellets were then resuspended either in 10 μL of TPM (for nonfluorophore controls) or 10 μL of DBCO-fluorophore solution (30 μM stock solution prepared in TPM). Resuspended cells were incubated in the dark with rocking (170 rpm) at 37 °C for 30 min to promote SPAAC click chemistry reactions between DBCO and the -N_3 groups on Kdo analogues; the cells were then sedimented via centrifuge and washed twice with TPM as described above. For live-cell fluorescence microscopy of clicked cells, the final pellet was resuspended in 10 μL of CYE broth.

Single-Cell Motility and Fluorescence Analysis. For phase-contrast and fluorescence microscopy on agar pads, cells from (non)clicked samples were sedimented and resuspended in TPM buffer to OD_{600} 1.0, spotted (3 μL) on a glass coverslip, and then overlaid with a pad of 1.5% agar prepared with (TPM). For motility analysis, the cells were left to adhere for 15 min prior to imaging at 32 °C using an Axio Observer 7 fluorescence microscope (Zeiss) with a 40× Plan Apochromat 1.3 oil objective VIS-IR M27 for single-cell motility and objective α Plan-Apochromat 100×/1.46 Oil DIC (UV) M27 for fluorescence analysis, with Axiocam 512 camera, TL LED as light source, and Zen Black software (Zeiss). DBCO-AF488 fluorescence was imaged using the 38 green fluorescent protein reflector, filter excitation wavelength 450−490, and filter emission wavelength 500−550. DBCO-TxRed fluorescence was imaged using the 92 HE/DAPI/GFP/mCherry reflector, filter excitation wavelength 583−600, and filter emission wavelength 617−758. DBCO-Cy5 fluorescence was imaged using the 50 Cy5 reflector, filter excitation wavelength 625−655, and filter emission wavelength 665−715. Images for single-cell gliding speed analysis were taken at 45 s intervals for 62 frames. Cell gliding speeds were calculated using the MicrobeJ module for Fiji.[37] Images for fluorescence analysis were taken at 30 s intervals. Gliding cell montages were generated using Fiji.

Cell Length Analysis. Images to be analyzed for cell length were acquired as part of the initial frames for the movies acquired for the determination of gliding speed (see above). Prior to analysis, images were processed in FIJI to optimize cell detection via the "Enhance Contrast" function (0.3%), followed by background subtraction (Rolling ball radius: 10.0

pixels, light background). Cells were measured using the FIJI MicrobeJ module.[37] The parameters used for length detection were set to "Basic", with the "MaxEntropy" method applied to threshold the images. The area selected for cell detection was set to 2−15 μm. Automatically detected objects were manually curated to remove any selections that were either background artifacts or merged cells to ensure only individual cells were analyzed. The length of each detected and retained object was then recorded in the results panel under the column "SHAPE.length" in micrometers.

Autoaggregation Testing. Real-time autoaggregation analysis was carried out as previously described.[13] In brief, for WT cells grown with(out) 7-N_3-Kdo, resuspensions from 10 mL cultures (grown for 24 h) were adjusted to OD_{600} 0.5 in CYE medium, with 1 mL of this resuspension transferred to a disposable spectrophotometer cuvette. Samples were strongly aspirated/ejected in the cuvette for 10 s via micropipette, followed by immediate OD_{600} determination (t = 0). Subsequent OD_{600} values were read every 10 min thereafter, up to 90 min. Cuvettes were covered and left undisturbed in a cuvette box atop the lab bench in between time points. All OD_{600} values were normalized against the initial OD_{600} reading obtained at t = 0 for each sample.

KdsB Enzyme Analysis of Kdo Azido Analogues. *Corynebacterium glutamicum* R163 harboring the expression plasmid pJKB72 was used to produce KdsB from *Escherichia coli* K-12 fused to a C-terminal histidine tag.[38] Protein was produced and purified through immobilized metal ion affinity chromatography using the protocol described by Mamat and co-workers.[39] The preparation was dialyzed (MWCO 6−8 kDa membrane) against Tris-HCl (20 mM) pH 7.5, NaCl (100 mM), $MgCl_2$ (5 mM), and 2-mercaptoethanol (2 mM) at 4 °C and concentrated with a centrifugal filter (MWCO 10 kDa). Protein was quantified with the Bradford protein assay and purity (>95%) was evaluated with a 12% SDS-PAGE gel. The final preparation was stored at −80 °C. To monitor KdsB enzymatic activity to evaluate Kdo azido analogues as potential substrates or inhibitors, we relied on the eikenogen assay described by Yi and co-workers.[30] This colorimetric assay quantifies pyrophosphate (PP_i) in the reaction mixture. The assay was performed in a 96-well clear, round bottom polystyrene microplate format. The reaction buffer consisted of glycine−NaOH (100 mM) pH 10.0 and $MgCl_2$ (5 mM). First, 10 μL of KdsB and 10 μL of Kdo/Kdo azido analogues in reaction buffer were added to the corresponding wells and preincubated for 10 min at room temperature. Then, 20 μL of CTP in reaction buffer was added. Each reaction mixture (40 μL) contained 100 nM KdsB and varying concentrations of CTP, Kdo, and Kdo azido analogues. The reaction was incubated at room temperature for the indicated times and an equal volume (40 μL) of ice-cold absolute ethanol was added to quench the reaction. Then, assay reagents were added as reported and the plate was incubated at room temperature for 20 min to allow color to develop. Absorbance was measured at 595 nm. Data were fitted to the Michaelis−Menten model using nonlinear regression.

Genomic Analyses. A dataset of 3,662 reference bacterial genomes was downloaded using the Prokaryotes.txt file on 2021-12-07 from NCBI. The Translated CDS files belonging to phylum Proteobacteria were subjected to offline hmmscan (E-value cutoff of 1×10^{-5}) against the Pfam-A v34.0 database (downloaded: 2021-03-24), followed by parsing via hmmscan-parser.sh, and arranging in the form of protein architecture

using in-house scripts. KdsB proteins were identified using the Pfam domain CTP_transf_3 (PF02348). From the total output, 38 KdsB proteins were selected from well-known organisms belonging to the phylum Proteobacteria. Alignments were performed using MUSCLE[40] and alignment was visualized using CHROMA.[41]

The NanT protein from *E. coli* (P41036.2) was used as a query to search for homologs in the *M. xanthus* genome using an *E*-value cutoff of 1×10^{-5}, which led to the identification of five NanT homologs in *M. xanthus* DZ2. Translated CDS files were subjected to offline hmmscan (*E*-value cutoff of 1×10^{-5}) against the Pfam-A v34.0 database, followed by parsing via hmmscan-parser.sh, and arranging in the form of protein architecture using in-house scripts. Proteins with Pfam domains MFS_1 (PF07690), MFS_1_like (PF12832), MFS_2 (PF13347), MFS_3 (PF05977), MFS_4 (PF06779), and MFS_5 (PF05631) associated with MFS transporters were identified from this output, leading to the identification of 31 putative MFS proteins.

■ ASSOCIATED CONTENT

Ⓢ Supporting Information

The Supporting Information is available free of charge at https://pubs.acs.org/doi/10.1021/acsomega.2c03711.

> Putative MFS transporters identified in *M. xanthus* with associated RNAseq transcriptomic profiling over the course of development (Table S1) (XLSX)

> ^{1}H NMR spectrum and negative-mode ESI MS of the *M. xanthus* DZ2 LPS O-antigen and core (Figure S1); TLC plates showing SPAAC reactivity of 8-N$_3$-Kdo and 7-N$_3$-Kdo (Figures S2 and S3); KdsB binding pocket containing CTP and 2-deoxy-Kdo (Figure S4); multiple sequence alignment of proteobacterial KdsB sequence homologues (Figure S5); assorted ^{1}H, ^{13}C, COSY, and HSQC NMR spectra for all novel synthesized compounds (Figures S6–S33) (PDF)

■ AUTHOR INFORMATION

Corresponding Authors

Charles Gauthier − *Institut National de la Recherche Scientifique (INRS)−Centre Armand-Frappier Santé Biotechnologie (AFSB), Université du Québec, Institut Pasteur International Network, Laval, Quebec H7V 1B7, Canada; Unité Mixte de Recherche INRS-UQAC, INRS−Centre AFSB, Université du Québec à Chicoutimi (UQAC), Chicoutimi, Quebec G7H 2B1, Canada;* orcid.org/0000-0002-2475-2050; Email: charles.gauthier@inrs.ca

Salim T. Islam − *Institut National de la Recherche Scientifique (INRS)−Centre Armand-Frappier Santé Biotechnologie (AFSB), Université du Québec, Institut Pasteur International Network, Laval, Quebec H7V 1B7, Canada; PROTEO, the Quebec Network for Research on Protein Function, Engineering, and Applications, Université Laval, Quebec, Quebec G1V 0A6, Canada;* orcid.org/0000-0001-6853-8446; Email: salim.islam@inrs.ca

Authors

Fares Saïdi − *Institut National de la Recherche Scientifique (INRS)−Centre Armand-Frappier Santé Biotechnologie (AFSB), Université du Québec, Institut Pasteur International Network, Laval, Quebec H7V 1B7, Canada; PROTEO, the Quebec Network for Research on Protein Function, Engineering, and Applications, Université Laval, Quebec, Quebec G1V 0A6, Canada*

Oscar Javier Gamboa Marin − *Institut National de la Recherche Scientifique (INRS)−Centre Armand-Frappier Santé Biotechnologie (AFSB), Université du Québec, Institut Pasteur International Network, Laval, Quebec H7V 1B7, Canada; Unité Mixte de Recherche INRS-UQAC, INRS−Centre AFSB, Université du Québec à Chicoutimi (UQAC), Chicoutimi, Quebec G7H 2B1, Canada*

José Ignacio Veytia-Bucheli − *Department of Chemistry, Laboratory of Bio-Organic Chemistry−Namur Research Institute for Life Sciences (NARILIS), University of Namur (UNamur), Namur 5000, Belgium;* orcid.org/0000-0003-4165-2884

Evgeny Vinogradov − *Vaccine Program, Human Health Therapeutics Portfolio, National Research Council, Ottawa, Ontario K1A 0R6, Canada;* orcid.org/0000-0002-5364-1376

Gokulakrishnan Ravicoularamin − *Institut National de la Recherche Scientifique (INRS)−Centre Armand-Frappier Santé Biotechnologie (AFSB), Université du Québec, Institut Pasteur International Network, Laval, Quebec H7V 1B7, Canada; Unité Mixte de Recherche INRS-UQAC, INRS−Centre AFSB, Université du Québec à Chicoutimi (UQAC), Chicoutimi, Quebec G7H 2B1, Canada*

Nicolas Y. Jolivet − *Institut National de la Recherche Scientifique (INRS)−Centre Armand-Frappier Santé Biotechnologie (AFSB), Université du Québec, Institut Pasteur International Network, Laval, Quebec H7V 1B7, Canada; PROTEO, the Quebec Network for Research on Protein Function, Engineering, and Applications, Université Laval, Quebec, Quebec G1V 0A6, Canada*

Ahmad A. Kezzo − *Institut National de la Recherche Scientifique (INRS)−Centre Armand-Frappier Santé Biotechnologie (AFSB), Université du Québec, Institut Pasteur International Network, Laval, Quebec H7V 1B7, Canada; PROTEO, the Quebec Network for Research on Protein Function, Engineering, and Applications, Université Laval, Quebec, Quebec G1V 0A6, Canada;* orcid.org/0000-0002-6502-2847

Eric Ramirez Esquivel − *Institut National de la Recherche Scientifique (INRS)−Centre Armand-Frappier Santé Biotechnologie (AFSB), Université du Québec, Institut Pasteur International Network, Laval, Quebec H7V 1B7, Canada; PROTEO, the Quebec Network for Research on Protein Function, Engineering, and Applications, Université Laval, Quebec, Quebec G1V 0A6, Canada*

Adyasha Panda − *Institute of Bioinformatics and Applied Biotechnology (IBAB), Bengaluru, Karnataka 560100, India*

Gaurav Sharma − *Institute of Bioinformatics and Applied Biotechnology (IBAB), Bengaluru, Karnataka 560100, India*

Stéphane P. Vincent − *Department of Chemistry, Laboratory of Bio-Organic Chemistry−Namur Research Institute for Life Sciences (NARILIS), University of Namur (UNamur), Namur 5000, Belgium;* orcid.org/0000-0001-6258-9058

Complete contact information is available at:
https://pubs.acs.org/10.1021/acsomega.2c03711

Author Contributions

S.T.I. and C.G. conceived and planned this study. O.J.G.M., G.R., and E.R.E. performed chemical synthesis of Kdo

■ ABBREVIATIONS USED

7-N$_3$-Kdo, 7-azido-7-deoxy-Kdo
8-N$_3$-Kdo, 8-azido-8-deoxy-Kdo
CMP, cytidine monophosphate
CTP, cytidine triphosphate
CuAAC, Cu(I)-catalyzed azide—alkyne cycloaddition
DBCO, dibenzocyclooctyne
DMSO, dimethylsulfoxide
EPS, exopolysaccharide
ESI—MS, electrospray ionization—mass spectrometry
GalNAc, *N*-acetyl-2-amino-2-deoxy-D-galactose
GalNAc6OMe, *N*-acetyl-2-amino-2-deoxy-6-*O*-methyl-D-galactose
GalNAc6P, *N*-acetyl-2-amino-2-deoxy-6-phosphoethyl-amine-D-galactose
Glc, D-glucose
Kdo, 3-deoxy-D-*manno*-oct-2-ulosonic acid
k_{cat}, turnover number
K_m, Michaelis constant
LPS, lipopolysaccharide
Man, D-mannose

MFS, major facilitator superfamily
NMR, nuclear magnetic resonance
OAg, O antigen
OD$_{600}$, optical density at 600 nm
OM, outer membrane
OS, oligosaccharide
*P*EtN, phosphoethanolamine
PP$_i$, pyrophosphate
SPAAC, strain-promoted azide—alkyne cycloaddition
T4P, type IV pili
TLC, thin-layer chromatography
WT, wild type
Xyl, D-xylose

■ REFERENCES

(1) Mitchell, A. M.; Silhavy, T. J. Envelope stress responses: balancing damage repair and toxicity. *Nat. Rev. Microbiol.* **2019**, *17*, 417−428.
(2) Bos, J.; Cisneros, L. H.; Mazel, D. Real-time tracking of bacterial membrane vesicles reveals enhanced membrane traffic upon antibiotic exposure. *Sci. Adv.* **2021**, *7*, eabd1033.
(3) Ducret, A.; Fleuchot, B.; Bergam, P.; Mignot, T. Direct live imaging of cell−cell protein transfer by transient outer membrane fusion in *Myxococcus xanthus*. *eLife* **2013**, *2*, e00868.
(4) Lam, J. S.; Taylor, V. L.; Islam, S. T.; Hao, Y.; Kocíncová, D. Genetic and functional diversity of *Pseudomonas aeruginosa* lipopolysaccharide. *Front. Microbiol.* **2011**, *2*, 1−25.
(5) Silipo, A.; Molinaro, A. The Diversity of the Core Oligosaccharide In Lipopolysaccharides. In *Endotoxins: Structure, Function and Recognition*, Wang, X.; Quinn, P. J., Eds.; Springer: Netherlands, 2010; pp 69−99.
(6) Goldman, R. C.; Kohlbrenner, W. E. Molecular cloning of the structural gene coding for CTP:CMP-3-deoxy-manno-octulosonate cytidylyltransferase from *Escherichia coli* K-12. *J. Bacteriol.* **1985**, *163*, 256−261.
(7) Dotson, G. D.; Dua, R. K.; Clemens, J. C.; Wooten, E. W.; Woodard, R. W. Overproduction and one-step purification of *Escherichia coli* 3-deoxy-D-manno-octulosonic acid 8-phosphate synthase and oxygen transfer studies during catalysis using isotopic-shifted heteronuclear NMR. *J. Biol. Chem.* **1995**, *270*, 13698−13705.
(8) Goldman, R. C.; Bolling, T. J.; Kohlbrenner, W. E.; Kim, Y.; Fox, J. L. Primary structure of CTP:CMP-3-deoxy-D-manno-octulosonate cytidylyltransferase (CMP-KDO synthetase) from *Escherichia coli*. *J. Biol. Chem.* **1986**, *261*, 15831−15835.
(9) Cambré, A.; Aertsen, A. Bacterial vivisection: how fluorescence-based imaging techniques shed a light on the inner workings of bacteria. *Microbiol. Mol. Biol. Rev.* **2020**, *84*, e00008-20.
(10) Dumont, A.; Malleron, A.; Awwad, M.; Dukan, S.; Vauzeilles, B. Click-mediated labeling of bacterial membranes through metabolic modification of the lipopolysaccharide inner core. *Angew. Chem. Int. Ed.* **2012**, *51*, 3143−3146.
(11) Fugier, E.; Dumont, A.; Malleron, A.; Poquet, E.; Mas Pons, J.; Baron, A.; Vauzeilles, B.; Dukan, S. Rapid and specific enrichment of culturable Gram negative bacteria using non-lethal copper-free click chemistry coupled with magnetic beads separation. *PLoS One* **2015**, *10*, e0127700.
(12) Vassen, V.; Valotteau, C.; Feuillie, C.; Formosa-Dague, C.; Dufrêne, Y. F.; De Bolle, X. Localized incorporation of outer membrane components in the pathogen *Brucella abortus*. *EMBO J.* **2019**, *38*, e100323.
(13) Saïdi, F.; Jolivet, N. Y.; Lemon, D. J.; Nakamura, A.; Belgrave, A. M.; Garza, A. G.; Veyrier, F. J.; Islam, S. T. Bacterial glycocalyx integrity drives multicellular swarm biofilm dynamism. *Mol. Microbiol.* **2021**, *116*, 1151−1172.
(14) Islam, S. T.; Vergara Alvarez, I.; Saïdi, F.; Guiseppi, A.; Vinogradov, E.; Sharma, G.; Espinosa, L.; Morrone, C.; Brasseur, G.; Guillemot, J.-F.; et al. Modulation of bacterial multicellularity via

spatio-specific polysaccharide secretion. *PLOS Biol.* **2020**, *18*, e3000728.

(15) Saïdi, F.; Mahanta, U.; Panda, A.; Kezzo, A. A.; Jolivet, N. Y.; Bitazar, R.; John, G.; Martinez, M.; Mellouk, A.; Calmettes, C.; et al. Bacterial outer-membrane polysaccharide export (OPX) proteins occupy three structural classes with selective *β*-barrel porin requirements for polymer secretion. *Microbiol. Spectr.* **2022**, DOI: 10.1128/spectrum.01290-22.

(16) Faure, L. M.; Fiche, J.-B.; Espinosa, L.; Ducret, A.; Anantharaman, V.; Luciano, J.; Lhospice, S.; Islam, S. T.; Tréguier, J.; Sotes, M.; et al. The mechanism of force transmission at bacterial focal adhesion complexes. *Nature* **2016**, *539*, 530−535.

(17) Islam, S. T.; Mignot, T. The mysterious nature of bacterial surface (gliding) motility: a focal adhesion-based mechanism in *Myxococcus xanthus*. *Semin. Cell Dev. Biol.* **2015**, *46*, 143−154.

(18) Pathak, D. T.; Wei, X.; Bucuvalas, A.; Haft, D. H.; Gerloff, D. L.; Wall, D. Cell contact−dependent outer membrane exchange in Myxobacteria: genetic determinants and mechanism. *PLoS Genet.* **2012**, *8*, e1002626.

(19) Vassallo, C.; Pathak, D. T.; Cao, P.; Zuckerman, D. M.; Hoiczyk, E.; Wall, D. Cell rejuvenation and social behaviors promoted by LPS exchange in myxobacteria. *Proc. Natl. Acad. Sci. U.S.A.* **2015**, *112*, E2939−E2946.

(20) MacLean, L.; Perry, M. B.; Nossova, L.; Kaplan, H.; Vinogradov, E. The structure of the carbohydrate backbone of the LPS from *Myxococcus xanthus* strain DK1622. *Carbohydr. Res.* **2007**, *342*, 2474−2480.

(21) Smellie, I. A.; Bhakta, S.; Sim, E.; Fairbanks, A. J. Synthesis of putative chain terminators of mycobacterial arabinan biosynthesis. *Org. Biomol. Chem.* **2007**, *5*, 2257−2266.

(22) Winzar, R.; Philips, J.; Kiefel, M. J. A simple synthesis of C-8 modified 2-keto-3-deoxy-D-manno-octulosonic acid (KDO) derivatives. *Synlett* **2010**, *4*, 583−586.

(23) Shirai, R.; Ogura, H. Improved syntheses of two 3-deoxyald-2-ulosonic acids (KDN, KDO) by condensation of oxalacetic acid with aldoses followed by Ni^{2+} catalyzed decarboxylation. *Tetrahedron Lett.* **1989**, *30*, 2263−2264.

(24) Müller, B.; Blaukopf, M.; Hofinger, A.; Zamyatina, A.; Brade, H.; Kosma, P. Efficient synthesis of 4-amino-4-deoxy-L-arabinose and spacer-equipped 4-amino-4-deoxy-L-arabinopyranosides by trans-glycosylation reactions. *Synthesis* **2010**, *2010*, 3143−3151.

(25) Bharathi, M. V.; Chhabra, M.; Paira, P. Development of surface immobilized 3-azidocoumarin-based fluorogenic probe via strain promoted click chemistry. *Bioorg. Med. Chem. Lett.* **2015**, *25*, 5737−5742.

(26) Nilsson, I.; Prathapam, R.; Grove, K.; Lapointe, G.; Six, D. A. The sialic acid transporter NanT is necessary and sufficient for uptake of 3-deoxy-D-*manno*-oct-2-ulosonic acid (Kdo) and its azido analog in *Escherichia coli*. *Mol. Microbiol.* **2018**, *110*, 204−218.

(27) Jain, R.; Habermann, B. H.; Mignot, T. Complete genome assembly of *Myxococcus xanthus* strain DZ2 using long high-fidelity (hifi) reads generated with PacBio technology. *Microbiol. Resour. Announc.* **2021**, *10*, e00530-21.

(28) Sharma, G.; Yao, A. I.; Smaldone, G. T.; Liang, J.; Long, M.; Facciotti, M. T.; Singer, M. Global gene expression analysis of the *Myxococcus xanthus* developmental time course. *Genomics* **2021**, *113*, 120−134.

(29) Muñoz-Dorado, J.; Moraleda-Muñoz, A.; Marcos-Torres, F. J.; Contreras-Moreno, F. J.; Martin-Cuadrado, A. B.; Schrader, J. M.; Higgs, P. I.; Pérez, J. Transcriptome dynamics of the *Myxococcus xanthus* multicellular developmental program. *eLife* **2019**, *8*, e50374.

(30) Yi, L.; Velasquez, M. S.; Holler, T. P.; Woodard, R. W. A simple assay for 3-deoxy-d-manno-octulosonate cytidylyltransferase and its use as a pathway screen. *Anal. Biochem.* **2011**, *416*, 152−158.

(31) Heyes, D. J.; Levy, C.; Lafite, P.; Roberts, I. S.; Goldrick, M.; Stachulski, A. V.; Rossington, S. B.; Stanford, D.; Rigby, S. E. J.; Scrutton, N. S.; Leys, D. Structure-based mechanism of CMP-2-keto-3-deoxymanno-octulonic acid synthetase. *J. Biol. Chem.* **2009**, *284*, 35514−35523.

(32) Nilsson, I.; Grove, K.; Dovala, D.; Uehara, T.; Lapointe, G.; Six, D. A. Molecular characterization and verification of azido-3,8-dideoxy-d-manno-oct-2-ulosonic acid incorporation into bacterial lipopoly-saccharide. *J. Biol. Chem.* **2017**, *292*, 19840−19848.

(33) Saïdi, F.; Bitazar, R.; Bradette, N.; Islam, S. T. Bacterial glycocalyx integrity impacts tolerance of *Myxococcus xanthus* to antibiotics and oxidative-stress agents. *Biomolecules* **2022**, *12*, 571.

(34) Cloutier, M.; Gauthier, C. Chapter Four-3-Deoxy-d-manno-oct-2-ulosonic acid (Kdo) derivatives in antibacterial drug discovery. In *Carbohydrates in Drug Discovery and Development*, Tiwari, V. K., Ed.; Elsevier: 2020; pp 155−212.

(35) Campos, J. M.; Zusman, D. R. Regulation of development in *Myxococcus xanthus*: effect of 3′:5′-cyclic AMP, ADP, and nutrition. *Proc. Natl. Acad. Sci. U. S. A.* **1975**, *72*, 518−522.

(36) Ducret, A.; Valignat, M.-P.; Mouhamar, F.; Mignot, T.; Theodoly, O. Wet-surface-enhanced ellipsometric contrast micros-copy identifies slime as a major adhesion factor during bacterial surface motility. *Proc. Natl. Acad. Sci. U.S.A.* **2012**, *109*, 10036−10041.

(37) Ducret, A.; Quardokus, E. M.; Brun, Y. V. MicrobeJ, a tool for high throughput bacterial cell detection and quantitative analysis. *Nat. Microbiol.* **2016**, *1*, 16077.

(38) Gronow, S.; Brabetz, W.; Brade, H. Comparative functional characterization in vitro of heptosyltransferase I (WaaC) and II (WaaF) from *Escherichia coli*. *Eur. J. Biochem.* **2000**, *267*, 6602−6611.

(39) Mamat, U.; Schmidt, H.; Munoz, E.; Lindner, B.; Fukase, K.; Hanuszkiewicz, A.; Wu, J.; Meredith, T. C.; Woodard, R. W.; Hilgenfeld, R.; et al. WaaA of the hyperthermophilic bacterium *Aquifex aeolicus* is a monofunctional 3-deoxy-d-manno-oct-2-ulosonic acid transferase involved in lipopolysaccharide biosynthesis. *J. Biol. Chem.* **2009**, *284*, 22248−22262.

(40) Edgar, R. C. MUSCLE: multiple sequence alignment with high accuracy and high throughput. *Nucl. Acids Res.* **2004**, *32*, 1792−1797.

(41) Goodstadt, L.; Ponting, C. P. CHROMA: consensus-based colouring of multiple alignments for publication. *Bioinformatics* **2001**, *17*, 845−846.

⬚ Recommended by ACS